Present status and future perspectives for neutrinoless double beta decay nuclear matrix elements

Tomás R. Rodríguez

International Workshop XLIII on Gross Properties of Nuclei and Nuclear Excitations

Hirschegg, January 15th, 2015

Acknowledgments

G. Martínez-Pinedo (TU-Darmstadt)

J. Menéndez (TU-Darmstadt/RIKEN)

N. López-Vaquero (UAM-Madrid)

J. L. Egido (UAM-Madrid)

A. Poves (UAM-Madrid)

Outline

1. Introduction
2. $0\nu\beta\beta$ transition operator
3. Nuclear structure effects
4. Summary and outlook

Neutrinoless double beta decay

Process mediated by the weak interaction which occurs in those even-even nuclei w… decay is energetically forb…

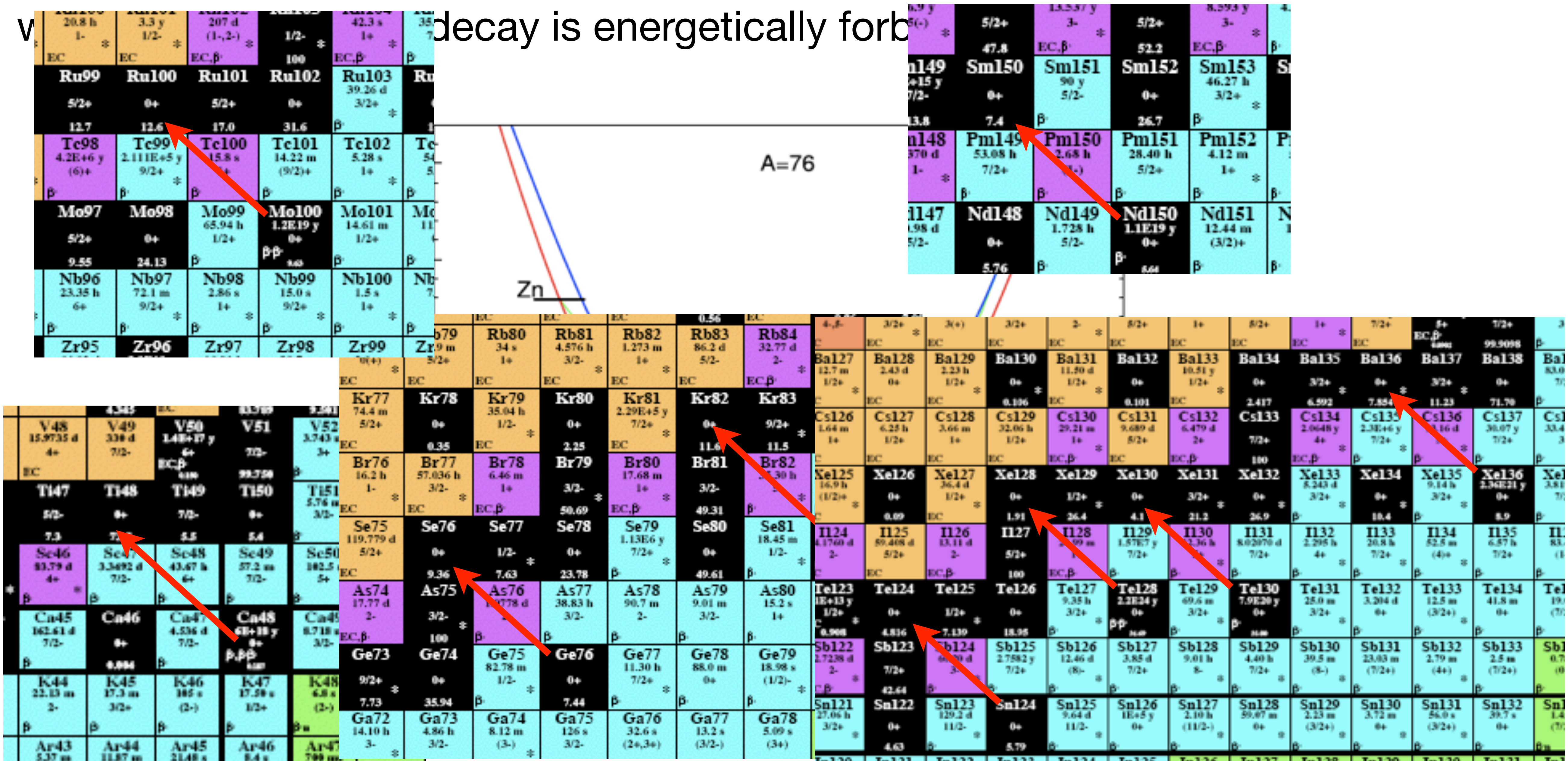

Neutrinoless double beta decay

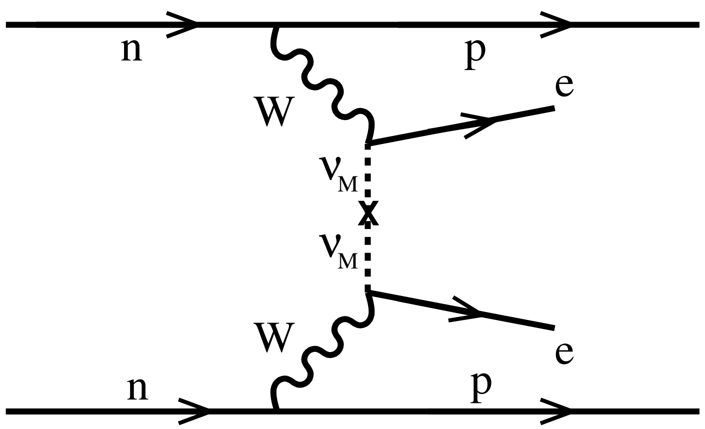

$$ {}^{A}_{Z}X_{N} \Rightarrow {}^{A}_{Z+2}Y_{N-2} + 2e^{-} $$

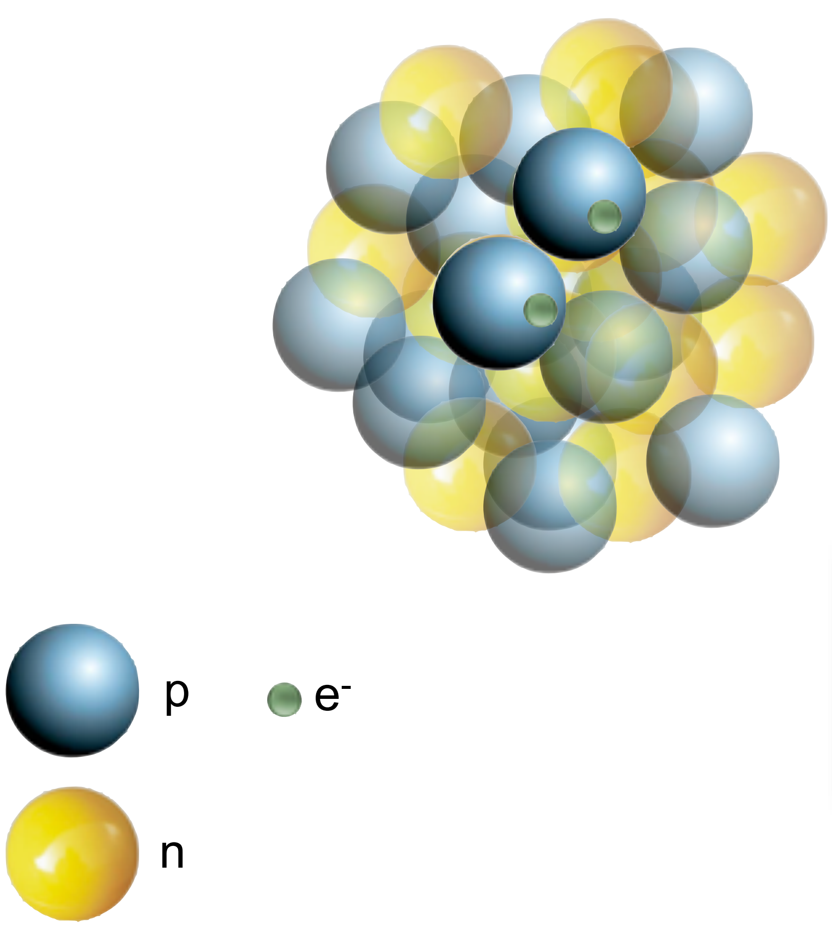

- Violates the leptonic number conservation
- Neutrinos are massive Majorana particles
- Mass hierarchy of neutrinos
- Experimentally not observed ($T_{1/2} > 10^{25}$ y)
- Beyond the Standard Model
- Most plausible mechanism: exchange of light Majorana neutrinos

$$ \left(T_{1/2}^{0\nu\beta\beta}(0^{+}\rightarrow 0^{+})\right)^{-1} = G_{01}\left|M^{0\nu\beta\beta}\right|^{2}\left(\frac{\langle m_{\beta\beta}\rangle}{m_e}\right)^{2} $$

Phase space factor

Nuclear Matrix Element

Phys. Rev. C 85, 034316 (2012).

Phys. Rev. C 88, 037303 (2013).

Current experimental status

UNIVERSIDAD AUTONOMA DE MADRID

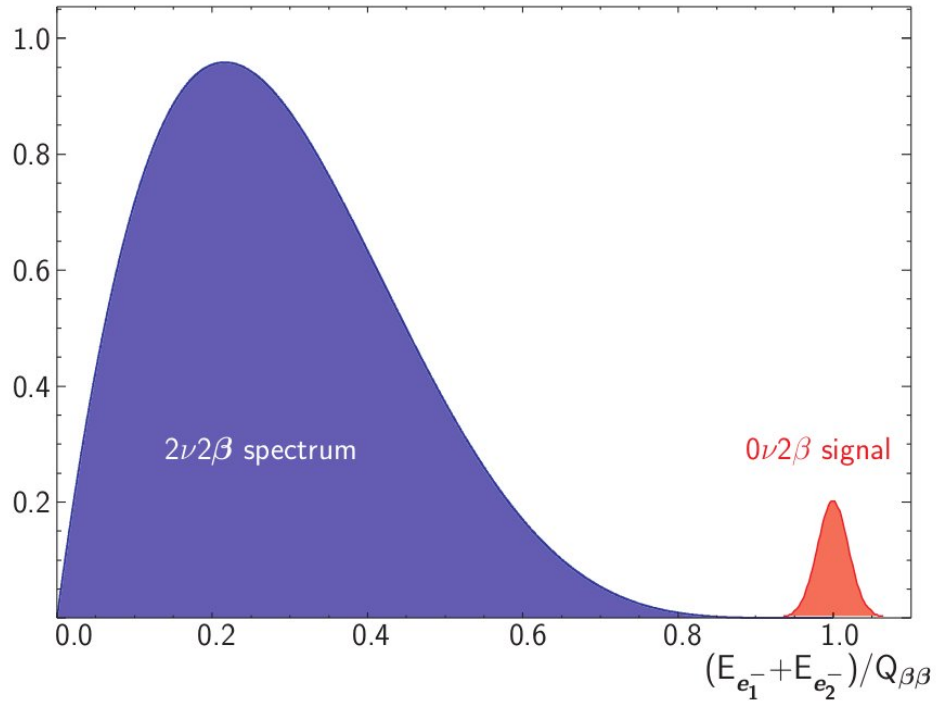

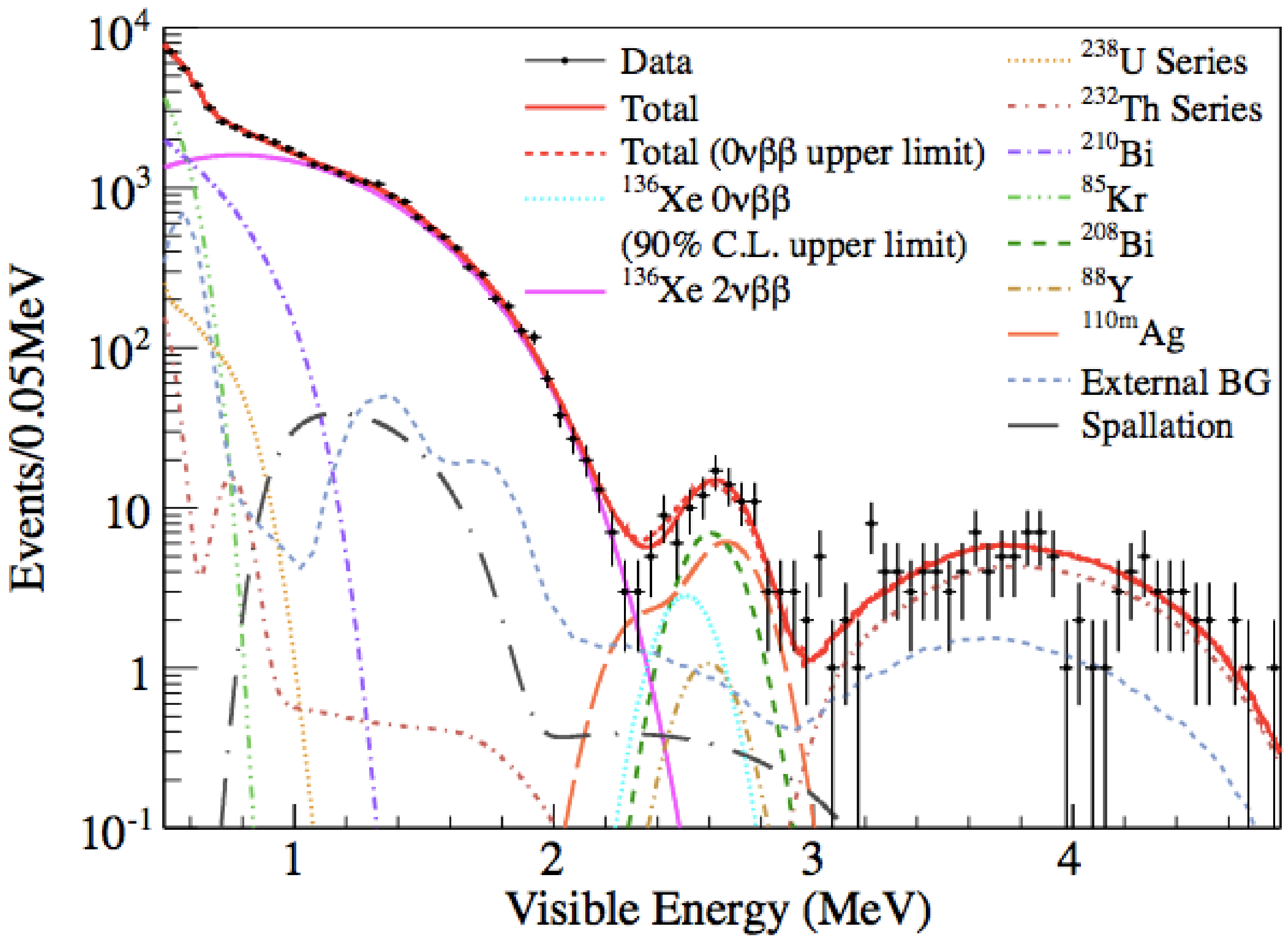

Only lower limits to the half-lives have been measured so far

- **KamLAND-Zen**, 370 kg (^{136}Xe)
- $T_{1/2} > 1.9 \times 10^{25}$ yr (90% C.L.)

PRL 110, 062502 (2013)

Current experimental status

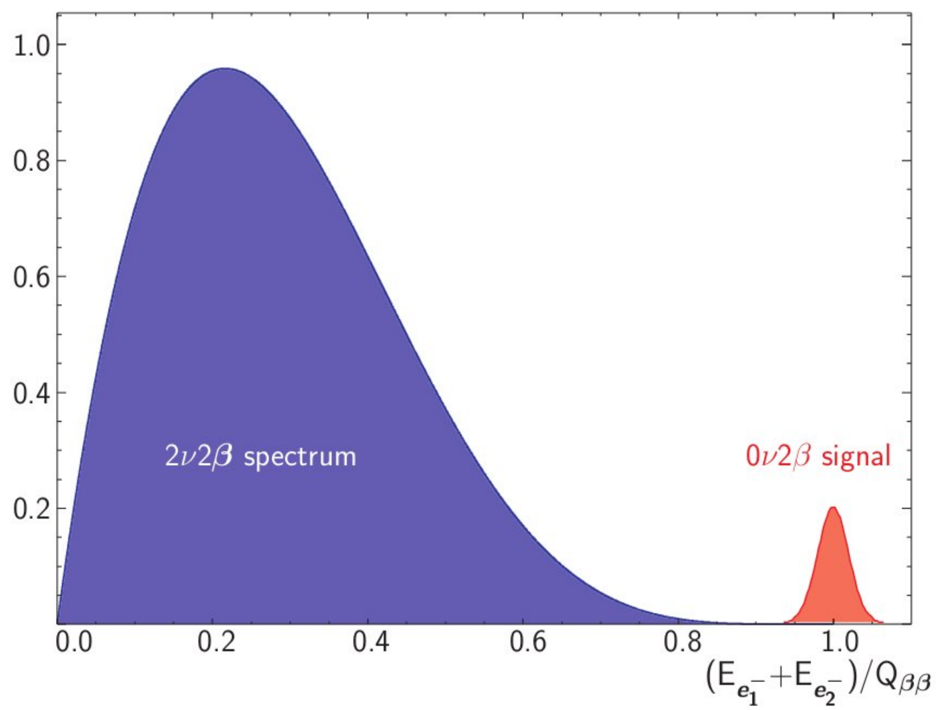

Only lower limits to the half-lives have been measured so far

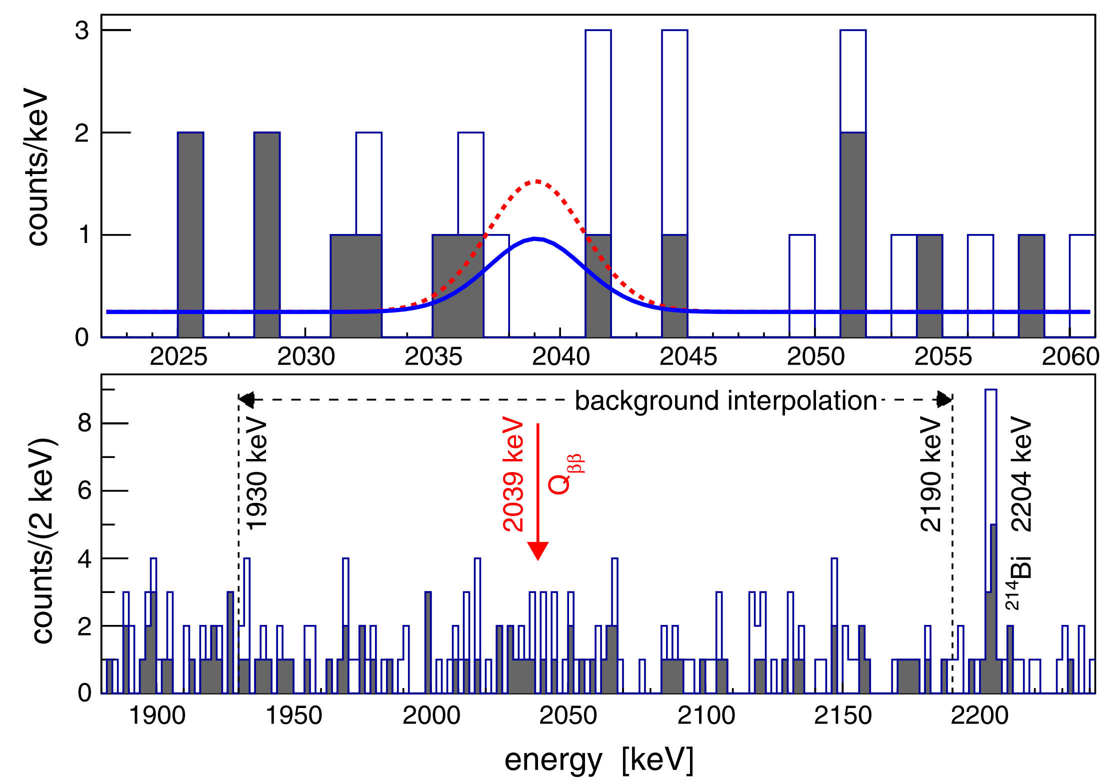

FIG. 1 (color online). The combined energy spectrum from all ^{enr}Ge detectors without (with) PSD is shown by the open (filled) histogram. The lower panel shows the region used for the background interpolation. In the upper panel, the spectrum zoomed to $Q_{\beta\beta}$ is superimposed with the expectations (with PSD selection) based on the central value of Ref. [11] $T_{1/2}^{0\nu} = 1.19 \times 10^{25}$ yr (red dashed) and with the 90% upper limit derived in this work, corresponding to $T_{1/2}^{0\nu} = 2.1 \times 10^{25}$ yr (blue solid).

- **GERDA**, exposure of 21 kg yr (^{76}Ge)
- $T_{1/2} > 2.1 \times 10^{25}$ yr (90% C.L.)
- Rules out HM claim

PRL 111, 122503 (2013)

Current experimental status

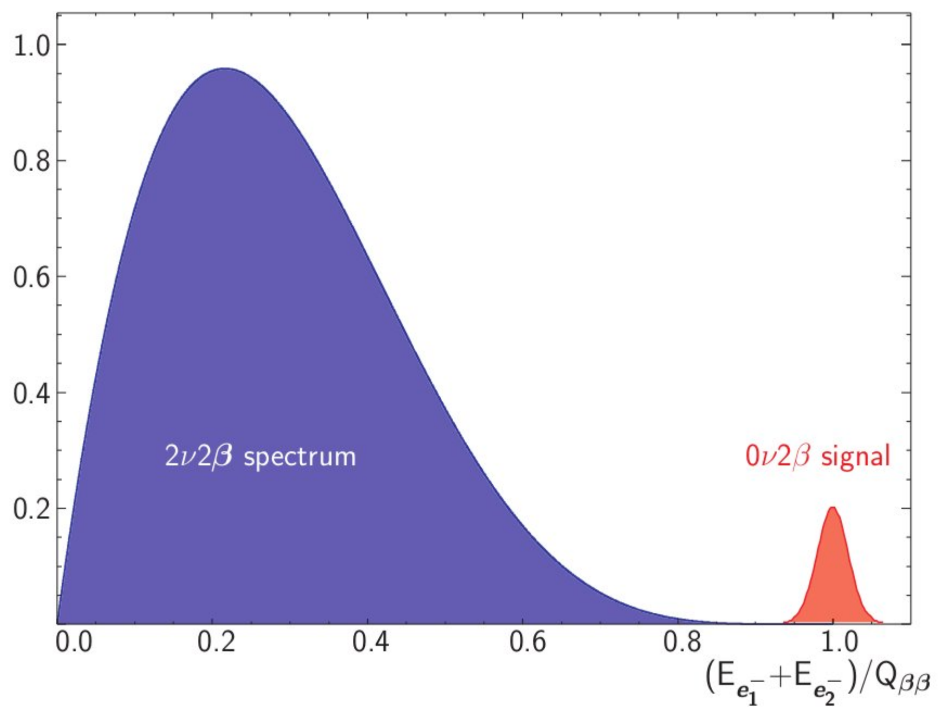

Only lower limits to the half-lives have been measured so far

- **EXO-200**, exposure of 100 kg yr (^{136}Xe)
- $T_{1/2} > 1.1 \times 10^{25}$ yr (90% C.L.)

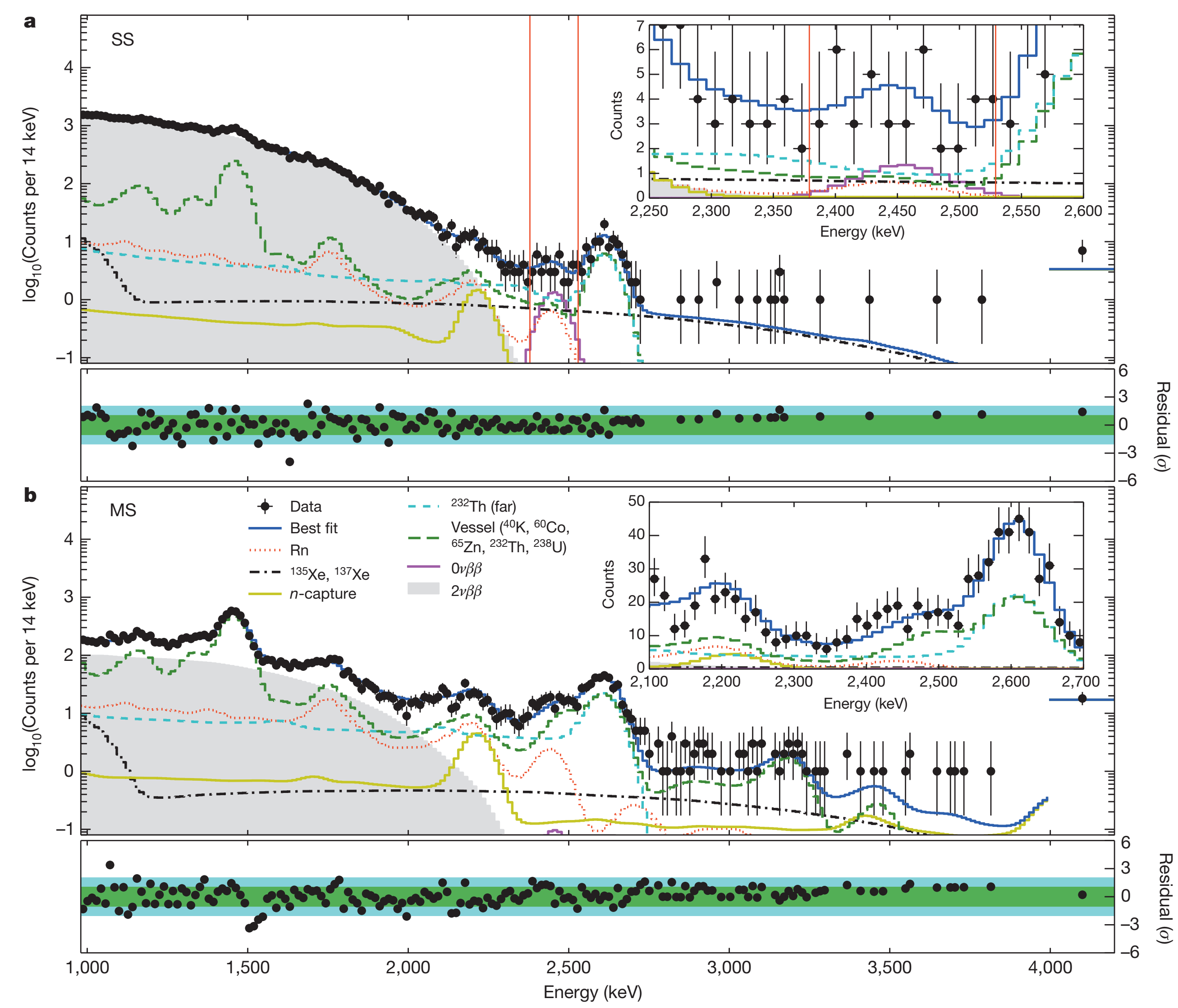

Figure 4 | Fit results projected in energy. **a**, **b**, Main panels show SS (**a**) and MS (**b**) events, as counts versus energy, with a zoom-in (inset) around the ROI: 2250–2600 keV (2100–2700 keV) for SS (MS); the bin size is 14 keV, and data points are shown in black. Lower panels in **a** and **b** show residuals between data and best fit normalized to the Poisson error, ignoring bins with 0 events. The green (blue) shaded regions in the lower panels represent $\pm1\sigma$ ($\pm2\sigma$) deviations. The 7 (18) events between 4,000 and 9,800 keV in the SS (MS) spectrum have been collected into an overflow bin for presentation here. The vertical (red) lines in the SS spectra indicate the $\pm2\sigma$ ROI. The result of the simultaneous fit to the standoff distance is not shown here. Several background model components (including Rn, ^{135}Xe and ^{137}Xe, *n*-capture, ^{232}Th (far), Vessel, $0\nu\beta\beta$ and $2\nu\beta\beta$, all described further in the text) are indicated in the main panel of **b** to show their relative contributions to the spectra. Error bars on data points, ±1 s.d.

Nature 510, 229 (2014)

Current experimental status

Experiment	Decay	Present limit $T_{1/2}$	Forecast limit $T_{1/2}$	Ref.
GERDA	^{76}Ge	> 2.1×10^{25} yr	~2×10^{26} yr	PRL. 111, 122503 (2013)
Majorana	^{76}Ge	— —	~4×10^{27} yr	arXiv:nucl-ex/ 0311013
EXO-200	^{136}Xe	> 1.1×10^{25} yr	~1.3×10^{28} yr	Nature 510, 229 (2014)
KamLAND-Zen	^{136}Xe	> 1.9×10^{25} yr	~4×10^{26} yr	PRL 110, 062502 (2013)
NEXT	^{136}Xe	— —	~10^{26} yr	JINST 7, C11007 (2012)
(Super)NEMO3	^{82}Se	> 3.6×10^{23} yr	~1.2×10^{26} yr	PRL 95, 182302 (2005)
CUORICINO (CUORE)	^{130}Te	> 3×10^{24} yr	~2×10^{26} yr	PRC 78, 035502 (2008)
(Super)NEMO3	^{150}Nd	> 1.8×10^{22} yr	~5×10^{25} yr	PRC 80, 032501 (2009)
SNO+	^{150}Nd	— —	> 1.6×10^{25} yr	J. Phys. Conf. Ser. 447, 012065 (2013)

COBRA: See Jan Tebruegge's talk!

Neutrino mass hierarchy

Neutrino flavor eigenstates are not the same as the mass eigenstates

$$U=\begin{pmatrix}\cos\theta_{12} & \sin\theta_{12} & 0\\ -\sin\theta_{12} & \cos\theta_{12} & 0\\ 0 & 0 & 1\end{pmatrix}\begin{pmatrix}\cos\theta_{13} & 0 & \sin\theta_{13}e^{-i\delta}\\ 0 & 1 & 0\\ -\sin\theta_{13}e^{i\delta} & 0 & \cos\theta_{13}\end{pmatrix}\begin{pmatrix}1 & 0 & 0\\ 0 & \cos\theta_{23} & \sin\theta_{23}\\ 0 & -\sin\theta_{23} & \cos\theta_{23}\end{pmatrix}\begin{pmatrix}1 & 0 & 0\\ 0 & e^{i\alpha_1} & 0\\ 0 & 0 & e^{i\alpha_1}\end{pmatrix}$$

solar reactor atmospheric

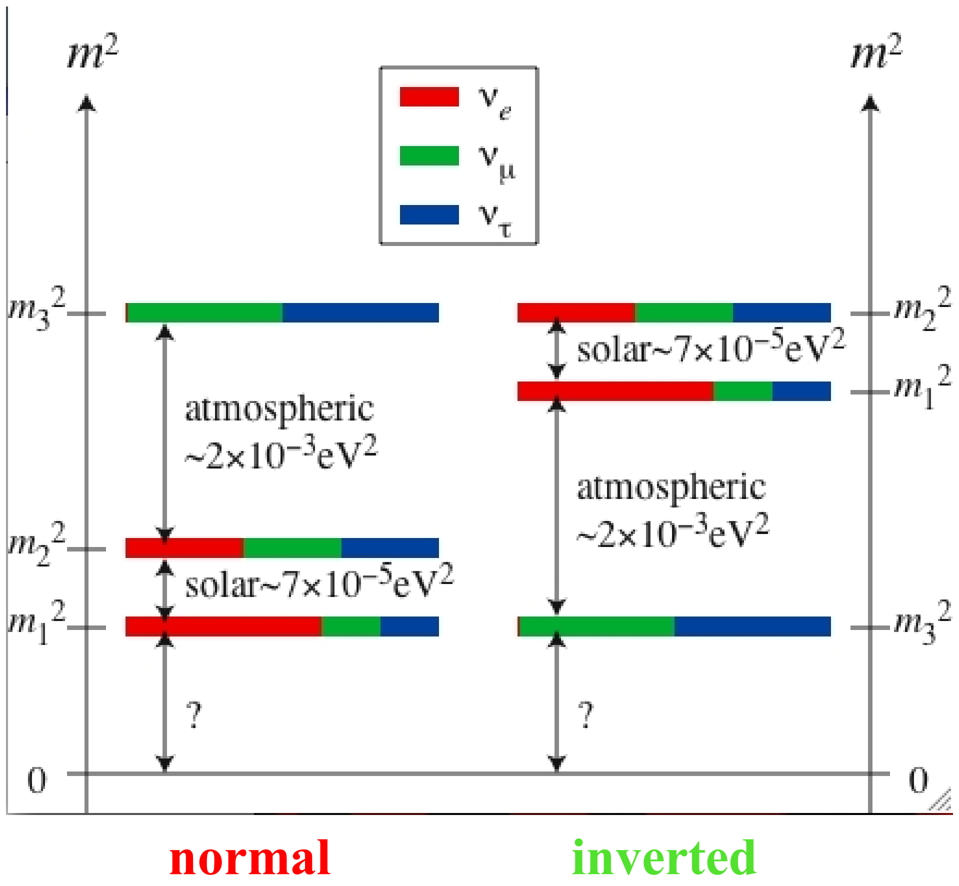

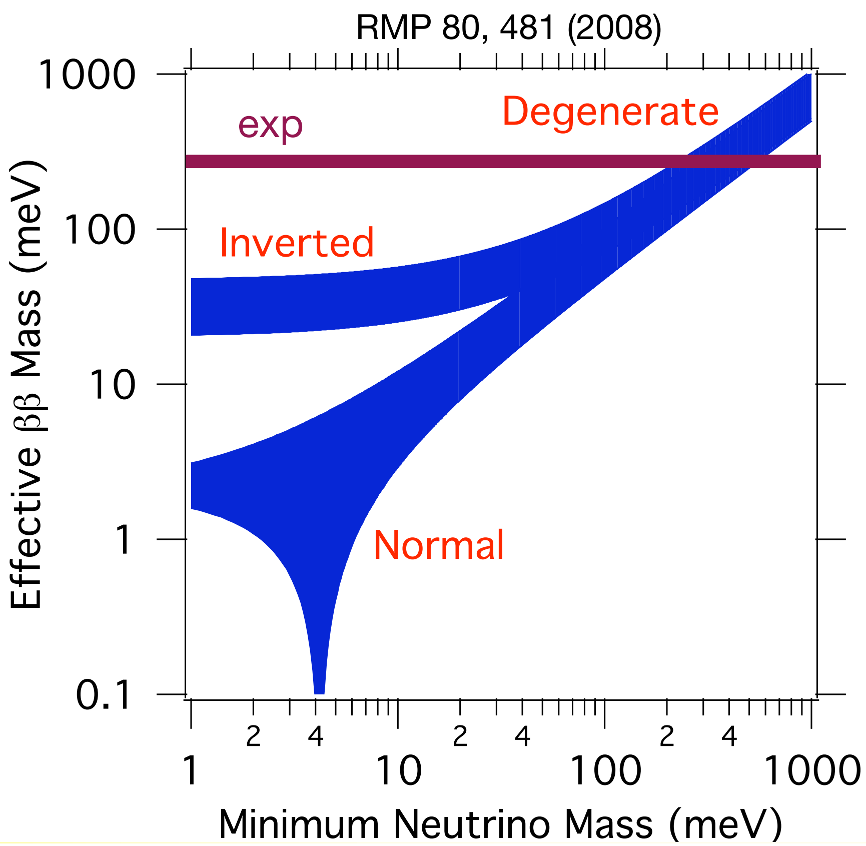

0νββ explores neutrino mass hierarchy and absolute mass scale

$$\langle m_{\beta\beta}\rangle=\sum_i U_{ei}^2 m_i$$

$$\left(T_{1/2}^{0\nu\beta\beta}(0^+\rightarrow 0^+)\right)^{-1}=G_{01}\left|M^{0\nu\beta\beta}\right|^2\left(\frac{\langle m_{\beta\beta}\rangle}{m_e}\right)^2$$

NME: Starting points

- Leading lepton number violating process contributing to $0\nu\beta\beta$ decay
  - **Exchange of light Majorana neutrino.**
  - Exchange of heavy Majorana neutrino.
  - Leptoquarks.
  - Supersymmetric particles.
  - …
- Transition operator connecting initial and final states
  - Relativistic/Non-relativistic.
  - Nucleon size effects.
  - Two-body weak currents.
  - Form factors.
  - Short-range correlations.
  - Closure approximation.
  - …
- Nuclear structure method (fully consistent or not with the operator) for calculating these NME.
  - Correlations.
  - Symmetry conservation.
  - Valence space.
  - …

Nuclear structure methods

Method	Recent references
Interacting Shell Model (ISM)	- Phys. Rev. Lett. 100, 052503 (2008). - Nucl. Phys. A 818, 139 (2009). - Phys. Rev. C 87, 014320 (2013). - Phys. Rev. Lett. 113, 262501 (2014).
pnQRPA	- Phys. Rev. C 77, 045503 (2008). - Phys Rev. C 87, 045501 (2013). - J. Phys. G 39, 124005 (2012).
Interacting Boson Model (IBM)	- Phys. Rev. C 79, 044301 (2009). - Phys Rev. C 87, 014315 (2013).
Generator Coordinate Method (GCM-EDF)	- Phys. Rev. Lett. 105, 252503 (2010). - Phys. Rev. Lett 111, 142501 (2013). - arXiv:1410.6326. - Phys. Rev. C 031031(R) (2014).

Current theoretical status

Different methods give different values of NME's with a factor ~3 difference

REDUCE THE UNCERTAINTIES:
- **EFFECTIVE OPERATOR**
- **NUCLEAR MANY-BODY METHOD (CORRELATIONS)**

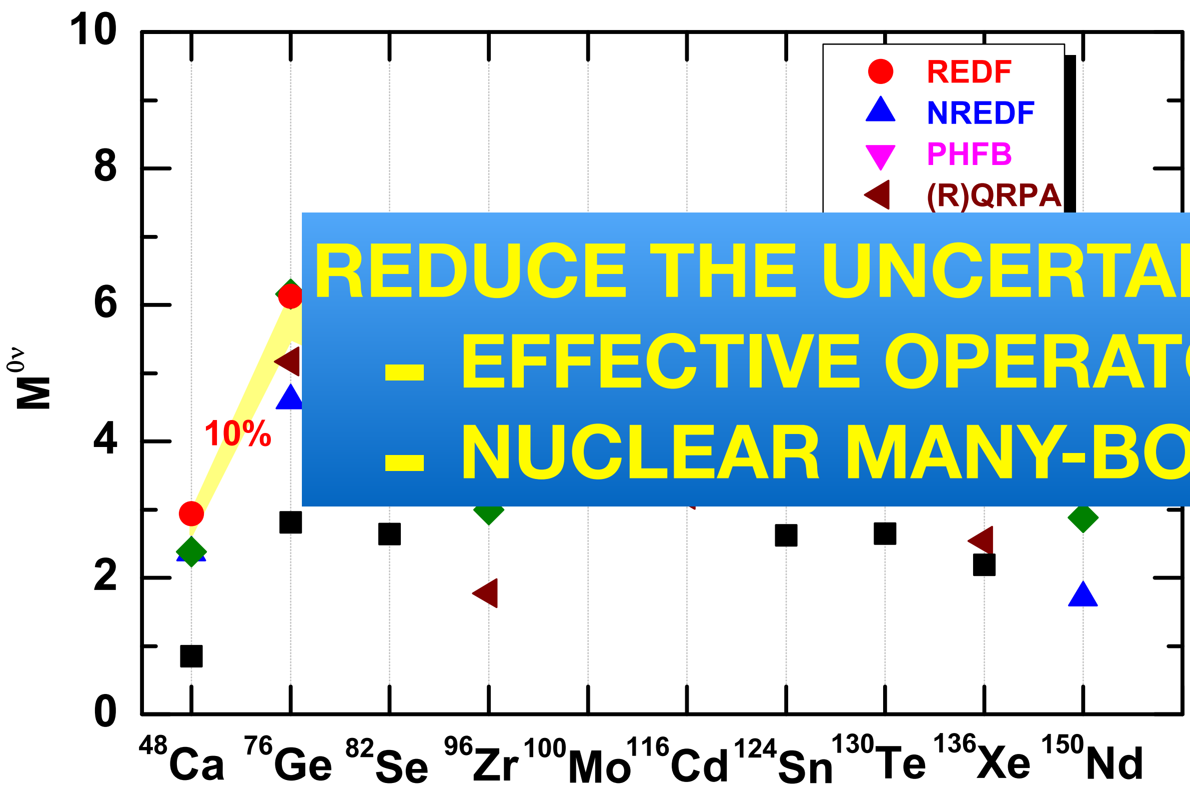

J. M. Yao et al., arXiv:1410.6326

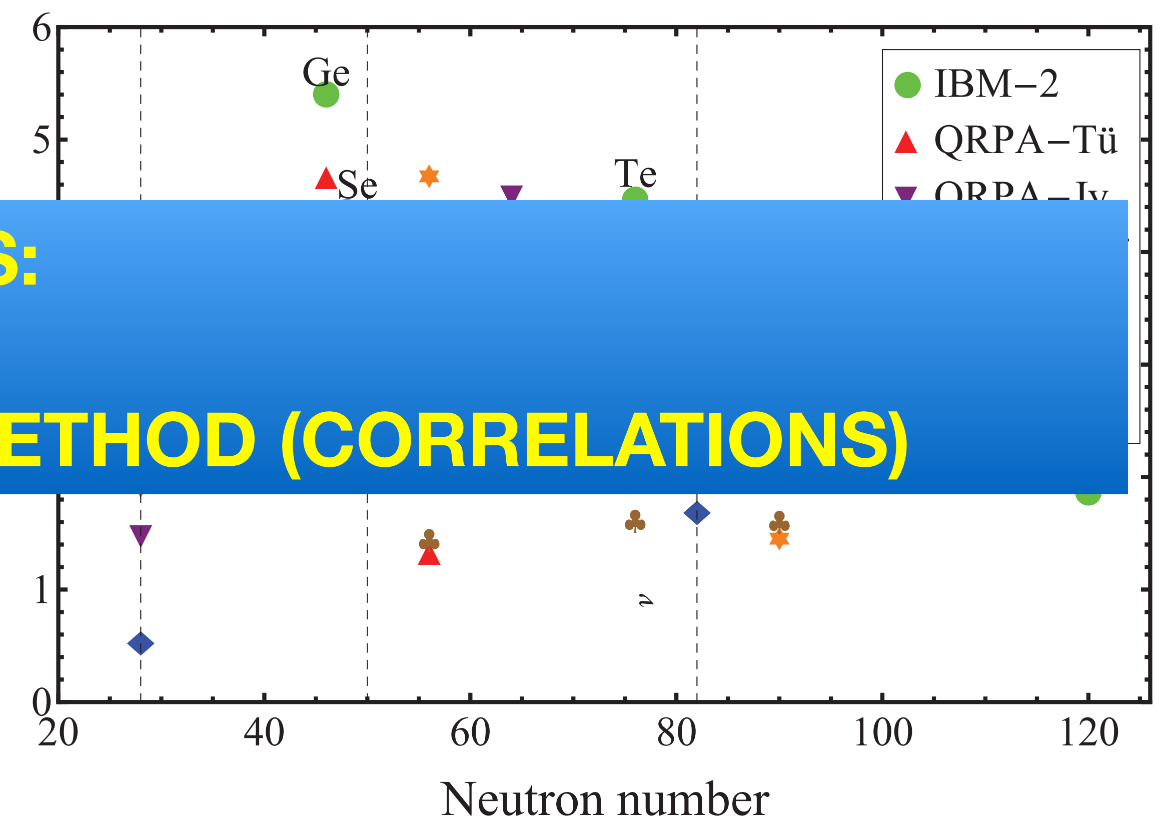

J. Barea, J. Kotila and F. Iachello, Phys. Rev. C 87, 014315 (2013)

Transition operator

- Relativistic form

$$\mathcal{H}_{\text{weak}}(x) = \frac{G_F \cos\theta_C}{\sqrt{2}} j^{\mu}(x)\mathcal{J}_{\mu}^{\dagger}(x) + \text{h.c.},$$

$$\hat{\mathcal{O}}^{0\nu} = \sum_i \hat{\mathcal{O}}_i^{0\nu}, \quad (i = VV, AA, AP, PP, MM)$$

$$j^{\mu}(x) = \bar{e}(x)\gamma^{\mu}(1 - \ldots$$

$$\ldots \frac{d^3q}{(2\pi)^3} \frac{\mathrm{e}^{\mathrm{i}\boldsymbol{q}\cdot(\boldsymbol{x}_1-\boldsymbol{x}_2)}}{q(q+E_d)} \left[\mathcal{J}_{\mu}^{\dagger}\mathcal{J}^{\mu\dagger}\right]_i$$

$$\mathcal{J}_{\mu}^{\dagger}(x) = \bar{\psi}(x)\Big[g_V(q^2) \ldots$$

$$- g_A(q^2)\gamma_{\mu}\gamma_5 - g_P(q^2)q_{\mu}\gamma_5\Big]\tau_-\psi(x),$$

$$\ldots \bar{\psi}\gamma^{\mu}\tau_-\psi)^{(2)},$$

$$g_A^2(\boldsymbol{q}^2)\left(\bar{\psi}\gamma_{\mu}\gamma_5\tau_-\psi\right)^{(1)}\left(\bar{\psi}\gamma^{\mu}\gamma_5\tau_-\psi\right)^{(2)},$$

$$2g_A(\boldsymbol{q}^2)g_P(\boldsymbol{q}^2)\left(\bar{\psi}\boldsymbol{\gamma}\gamma_5\tau_-\psi\right)^{(1)}\left(\bar{\psi}\boldsymbol{q}\gamma_5\tau_-\psi\right)^{(2)},$$

$$g_P^2(\boldsymbol{q}^2)\left(\bar{\psi}\boldsymbol{q}\gamma_5\tau_-\psi\right)^{(1)}\left(\bar{\psi}\boldsymbol{q}\gamma_5\tau_-\psi\right)^{(2)},$$

$$g_M^2(\boldsymbol{q}^2)\left(\bar{\psi}\frac{\sigma_{\mu i}}{2m_p}q^i\tau_-\psi\right)^{(1)}\left(\bar{\psi}\frac{\sigma^{\mu j}}{2m_p}q_j\tau_-\psi\right)^{(2)}.$$

$$M^{0\nu}(0_I^+ \to 0_F^+) \equiv \langle 0_F^+|\hat{\mathcal{O}}^{0\nu}|0_I^+\rangle,$$

Fully relativistic treatment:

L. S. Song et al., arXiv:1407.1368
J. M. Yao et al., arXiv:1410.6326

L. S. Song et al, arXiv:1407.1368

- Non-relativistic

$$M^{0\nu}(0^+_I \to 0^+_F)$$

$$\hat{\mathcal{O}}^{0\nu} = \sum_i \hat{\mathcal{O}}^{0\nu}_i, \quad (i =$$

$$\hat{\mathcal{O}}^{0\nu}_i = \frac{4\pi R}{g_A^2} \int d^3x_1 d^3x_2$$

r $[\mathcal{J}^\dagger_\mu \mathcal{J}^{\mu\dagger}]_{\rm NR}$ vistic calcula- nd the tensor

$\tau^{(1)}_- \tau^{(2)}_-$, (34)

$\boldsymbol{\sigma}^{(2)} \cdot \hat{\boldsymbol{q}}) - \sigma_{12}$: F, GT, T) the hadronic

$P, PP, MM)$

(35a)

(35b)

$\frac{\boldsymbol{q}^2}{2m_p}$, (35c)

(35d)

(35e)

(35f)

(35g)

(35h)

Table 1: The normalized NME $\tilde{M}^{0\nu}$ for the $0\nu\beta\beta$-decay obtained with the particle number projected spherical mean-field configuration ($\beta_I = \beta_F = 0$) by the PC-PK1 force using both the relativistic and non-relativistic reduced (first-order of q/m_p in the one-body current) transition operators. The ratio of the AA term to the total NME, $R_{AA} \equiv \tilde{M}^{0\nu}_{\rm AA}/\tilde{M}^{0\nu}$, the relativistic effect $\Delta_{\rm Rel.} \equiv (\tilde{M}^{0\nu} - \tilde{M}^{0\nu}_{\rm NR})/\tilde{M}^{0\nu}$ and the ratio of the tensor part to the total NME, $R_T \equiv \tilde{M}^{0\nu}_{\rm NR,T}/\tilde{M}^{0\nu}_{\rm NR}$, are also presented.

Sph+PNP (PC-PK1)	$\tilde{M}^{0\nu}$	R_{AA}	$\tilde{M}^{0\nu}_{\rm NR}$	$\Delta_{\rm Rel.}$	R_T
^{48}Ca $\to$ ^{48}Ti	3.66	81%	3.74	−2.1%	−2.4%
^{76}Ge $\to$ ^{76}Se	7.59	94%	7.71	−1.6%	3.5%
^{82}Se $\to$ ^{82}Kr	7.58	93%	7.68	−1.4%	2.9%
^{96}Zr $\to$ ^{96}Mo	5.64	95%	5.63	0.2%	3.6%
^{100}Mo $\to$ ^{100}Ru	10.92	95%	10.91	0.1%	3.5%
^{116}Cd $\to$ ^{116}Sn	6.18	94%	6.13	0.7%	1.9%
^{124}Sn $\to$ ^{124}Te	6.66	94%	6.78	−1.8%	4.9%
^{130}Te $\to$ ^{130}Xe	9.50	94%	9.64	−1.4%	4.3%
^{136}Xe $\to$ ^{136}Ba	6.59	94%	6.70	−1.7%	4.1%
^{150}Nd $\to$ ^{150}Sm	13.25	95%	13.08	1.3%	2.5%

J. M. Yao et al., arXiv:1410.6326

F. Simkovic et. al, PRC 60, 055502 (1999) L. S. Song et al, arXiv:1407.1368

Transition operator

- Non-relativistic reduction

- Neglect the tensor term.
- Closure approximation
(10% error at most, from QRPA and ISM calculations)

$$M^{0\nu\beta\beta} = -\left(\frac{g_V(0)}{g_A(0)}\right)^2 M_F^{0\nu\beta\beta} + M_{GT}^{0\nu\beta\beta} - \cancel{M_T^{0\nu\beta\beta}}$$

$$M_F^{0\nu\beta\beta} = \left(\frac{g_A(0)}{g_V(0)}\right)^2 \langle 0_f^+|\hat{V}_F(1,2)\hat{\tau}_-^{(1)}\hat{\tau}_-^{(2)}|0_i^+\rangle$$

$$M_{GT}^{0\nu\beta\beta} = \langle 0_f^+|\hat{V}_{GT}(1,2)\hat{\tau}_-^{(1)}\hat{\tau}_-^{(2)}|0_i^+\rangle$$

$$\langle \vec{r}_1\vec{r}_2|\hat{V}_F(1,2)|\vec{r}'_1\vec{r}'_2\rangle = v_F(|\vec{r}_1-\vec{r}_2|)\delta(\vec{r}_1-\vec{r}'_1)\delta(\vec{r}_2-\vec{r}'_2)$$

$$\langle \vec{r}_1\vec{r}_2|\hat{V}_{GT}(1,2)|\vec{r}'_1\vec{r}'_2\rangle = v_{GT}(|\vec{r}_1-\vec{r}_2|)\delta(\vec{r}_1-\vec{r}'_1)\delta(\vec{r}_2-\vec{r}'_2)\hat{\vec{\sigma}}^{(1)}\cdot\hat{\vec{\sigma}}^{(2)}$$

Neutrino potentials

Neutrino potentials

Starting from the weak lagrangian that describes the process some approximations are made:

1. Non-relativistic approach in the hadronic part.

2. Closure approximation in the virtual intermediate state

3. Nucleon form factors taken in the dipolar approximation.

4. Tensor contribution is neglected.

5. High order currents are included (HOC).

6. Short range correlations are included with an UCOM correlator.

- Find the initial and final 0^+ (and, in the no closure approximation, the intermediate) states
- Evaluate the transition operators between these states

Transition operator

- The ‘bare’ operator should be transformed into an ‘effective’ operator defined in the valence space

MBPT

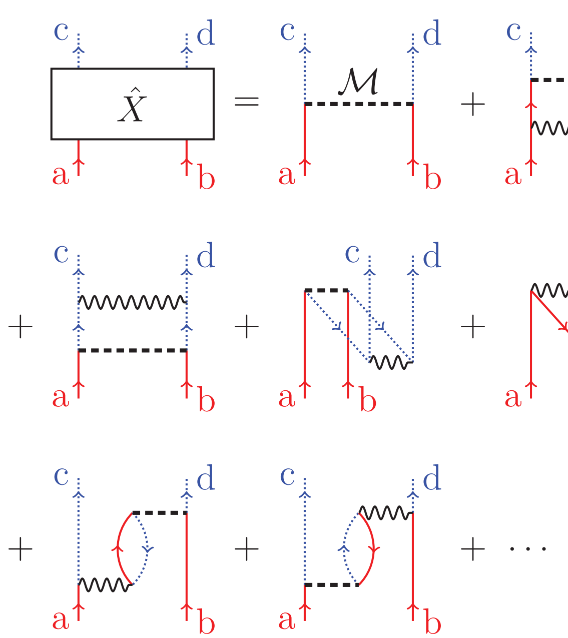

In-medium SRG could also do the job!

FIG. 2. (Color online) The $\hat{X}$ box to first order in $V_{\mathrm{low}\,k}$. Solid (red online) up- or down-going lines indicate neutrons and dotted (blue online) lines indicate protons. The wavy horizontal lines, as in Fig. 1, represent $V_{\mathrm{low}\,k}$, and the dashed horizontal lines represent the $0\nu\beta\beta$-decay operator in Eq. (1).

J.D. Holt, J. Engel, Phys. Rev. C 87, 064315 (2013)

- Two-body weak currents could play a relevant role

ISM

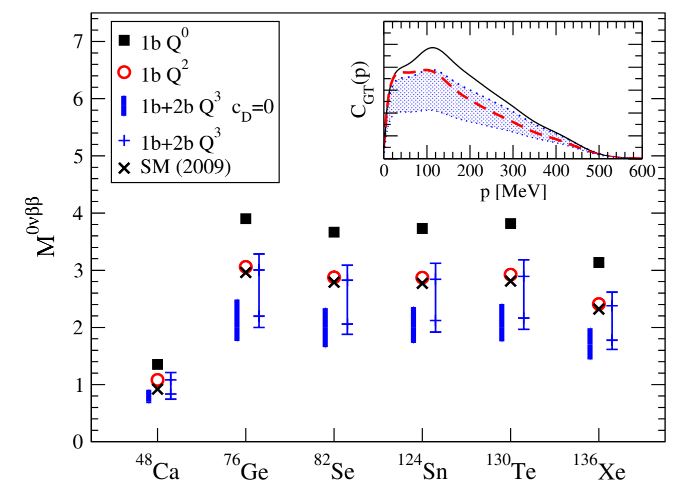

FIG. 2 (color online). Nuclear matrix elements $M^{0\nu\beta\beta}$ for $0\nu\beta\beta$ decay. At order Q^0, the NMEs include only the leading $p=0$ axial and vector $1b$ currents. At the next order, all Q^2 $1b$-current contributions not suppressed by parity are taken into account. At order Q^3, the thick bars are predicted from the long-range parts of $2b$ currents ($c_D=0$). The thin bars estimate the theoretical uncertainty from the short-range coupling c_D by taking an extreme range for the quenching (see text). For comparison, we show the SM results of Ref. [12] based on phenomenological $1b$ currents only. The inset (representative for ^{136}Xe) shows that the GT part, $M_{\mathrm{GT}}^{0\nu\beta\beta}=\int dp C_{\mathrm{GT}}(p)$, is dominated by $p\sim 100$ MeV.

J. Menéndez, D. Gazit, A. Schwenk, Phys. Rev. Lett. 107, 062501 (2011)

pnQRPA

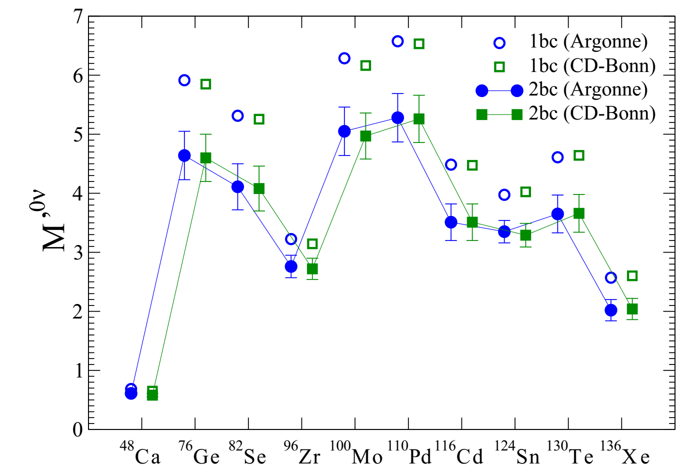

FIG. 1. (Color online) Nuclear matrix elements $M'^{0\nu}$ for all the nuclei considered here. The empty circles and squares represent the results with the one-body current only, and the solid circles and squares the average of the results with two-body currents included. The error bars represent the dispersion in those values (see text).

J. Engel, F. Simkovic, P. Vogel, Phys. Rev. C 89, 064308 (2014)

➥ these are problems closely related to the quenching of Gamow-Teller strength

NME: Nuclear structure aspects

We want to study the role of

- Deformation and shape mixing.
- Pairing pp/nn/pn correlations.
- Shell effects.
- Isospin conservation.
- Pair breaking (seniority).
- Occupation numbers.
- Size of the valence space.

in the nuclear matrix elements using a standard prescription for the transition operator.

Nuclear structure methods with phenomenological interactions

- Use of phenomenological interactions (adjusted to data in finite nuclei) is necessary to obtain precise predictions/descriptions of ground state, spectroscopic and reaction data.

SELF-CONSISTENT MEAN FIELD

- Variational approach with simple trial wave functions (HFB) using 'universal' functionals (applicable to the whole nuclear chart).
- Parameters of the functional fitted to bulk properties and masses and radii of finite nuclei.
- Very precise description of ground state properties and collective phenomena.
- Defined in the intrinsic frame.
- Spectroscopy and transitions with beyond-mean-field techniques (GCM, QRPA, …)

LARGE SCALE SHELL MODEL

- Exact diagonalizations within a valence space.
- Effective interactions adapted to the valence space and adjusted to reproduce the evolution of single particle energies (monopoles).
- Very precise description of spectroscopy and transitions of nuclei.
- Limited by the combinatorial increase of the number of configurations.
- Defined in the laboratory frame

Method: GCM+PNAMP

- **Effective nucleon-nucleon interaction:**

Gogny force (D1S-D1M) that is able to describe properly many phenomena along the whole nuclear chart.

$$V(1,2) = \sum_{i=1}^{2} e^{-(\vec{r}_1-\vec{r}_2)^2/\mu_i^2}\left(W_i + B_i P^\sigma - H_i P^\tau - M_i P^\sigma P^\tau\right)$$ central term

spin-orbit term $$+iW_0(\sigma_1+\sigma_2)\vec{k}\times\delta(\vec{r}_1-\vec{r}_2)\vec{k} + t_3(1+x_0P^\sigma)\delta(\vec{r}_1-\vec{r}_2)\rho^\alpha\left((\vec{r}_1+\vec{r}_2)/2\right)$$ density-dependent term

$$+V_{\mathrm{Coulomb}}(\vec{r}_1,\vec{r}_2)$$ Coulomb term

- **Method of solving the many-body problem:**

First step: Particle Number Projection (before the variation) of HFB-type wave functions.

Second step: Simultaneous **Particle Number and Angular Momentum Projection** (after the variation).

Third step: Configuration mixing within the framework of the **Generator Coordinate Method (GCM)**.

Particle number projection

Determination of initial and final states (I)

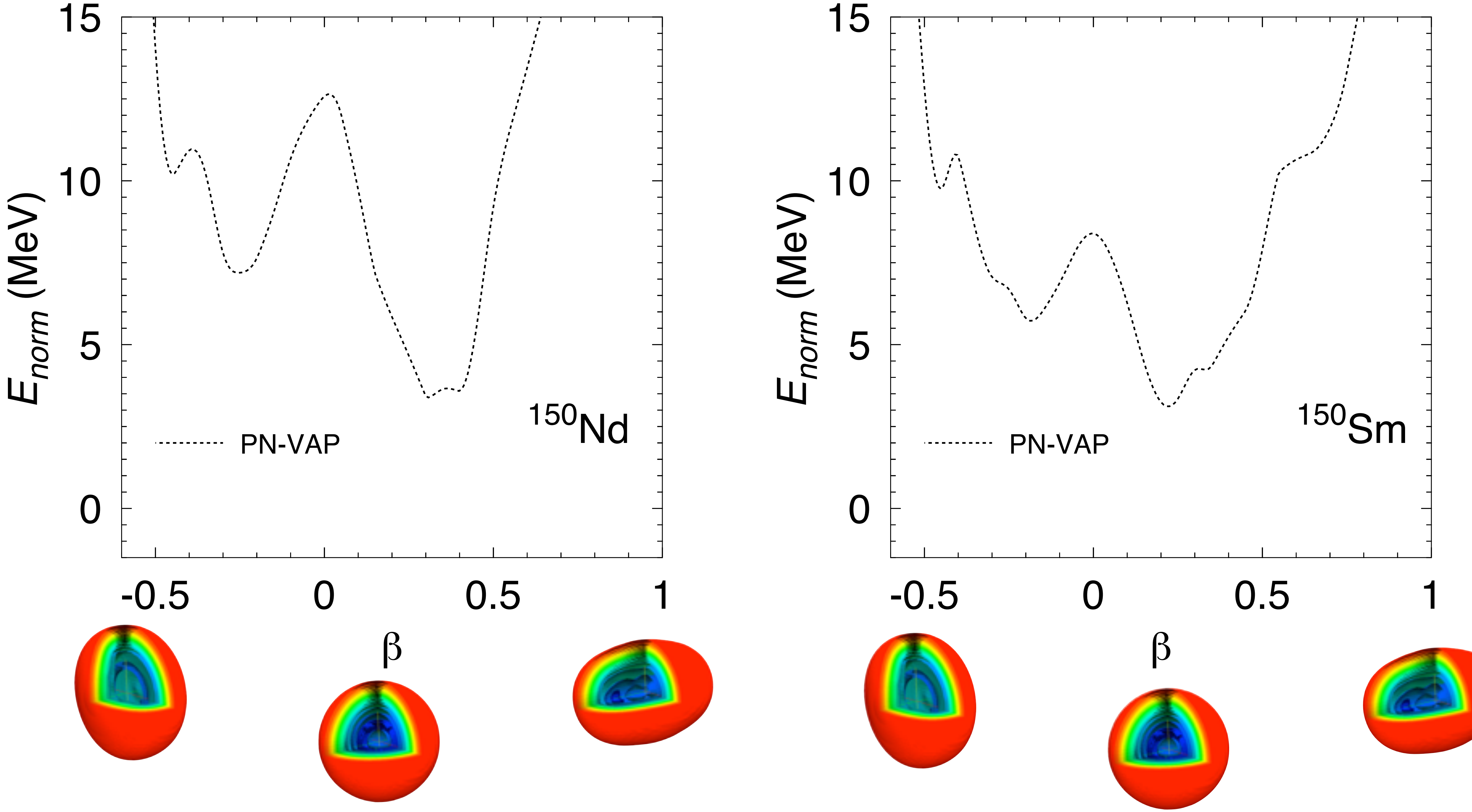

Particle number and angular momentum projection

Determination of initial and final states (II)

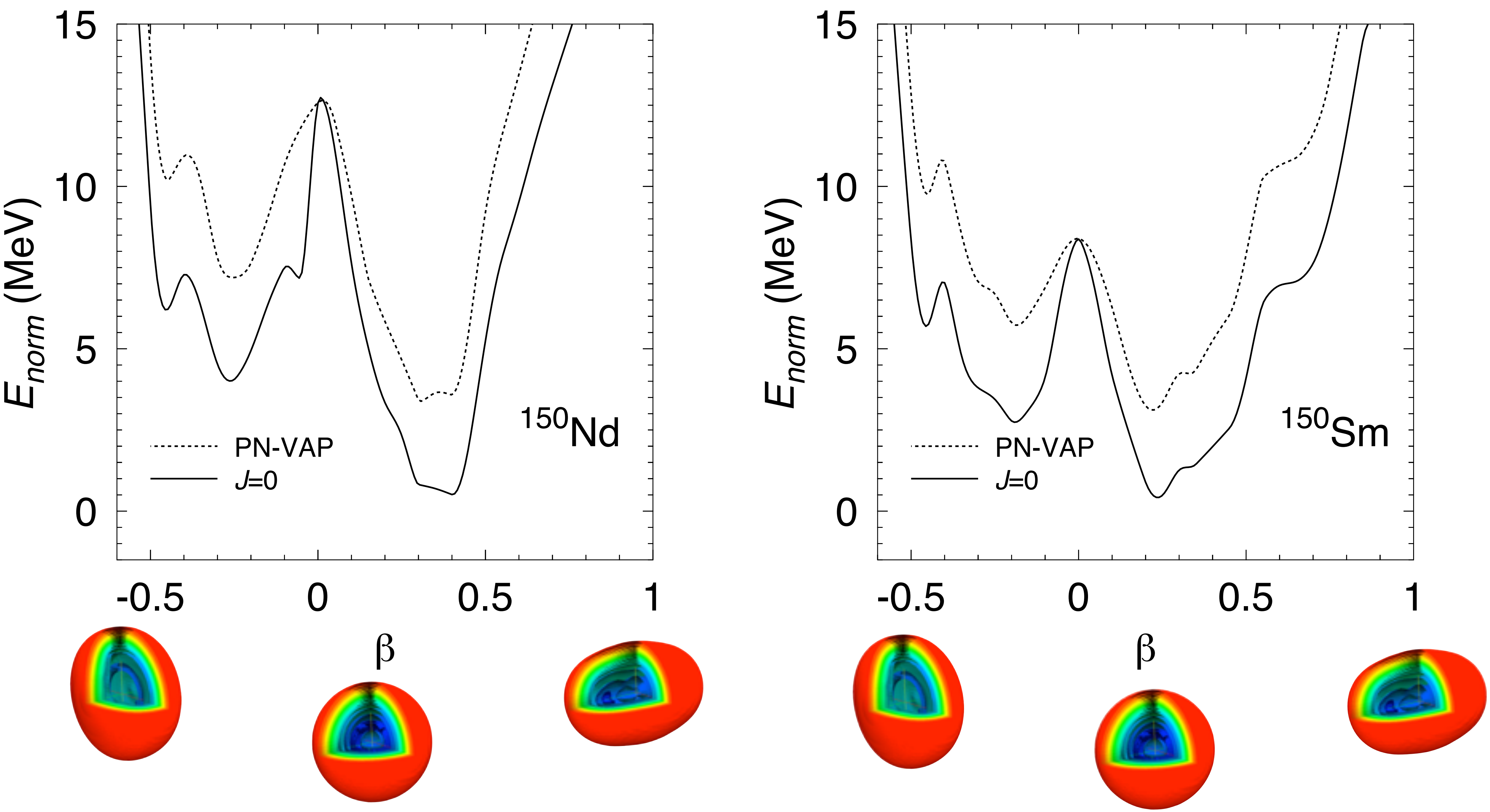

Configuration (shape) mixing

Determination of initial and final states (& III)

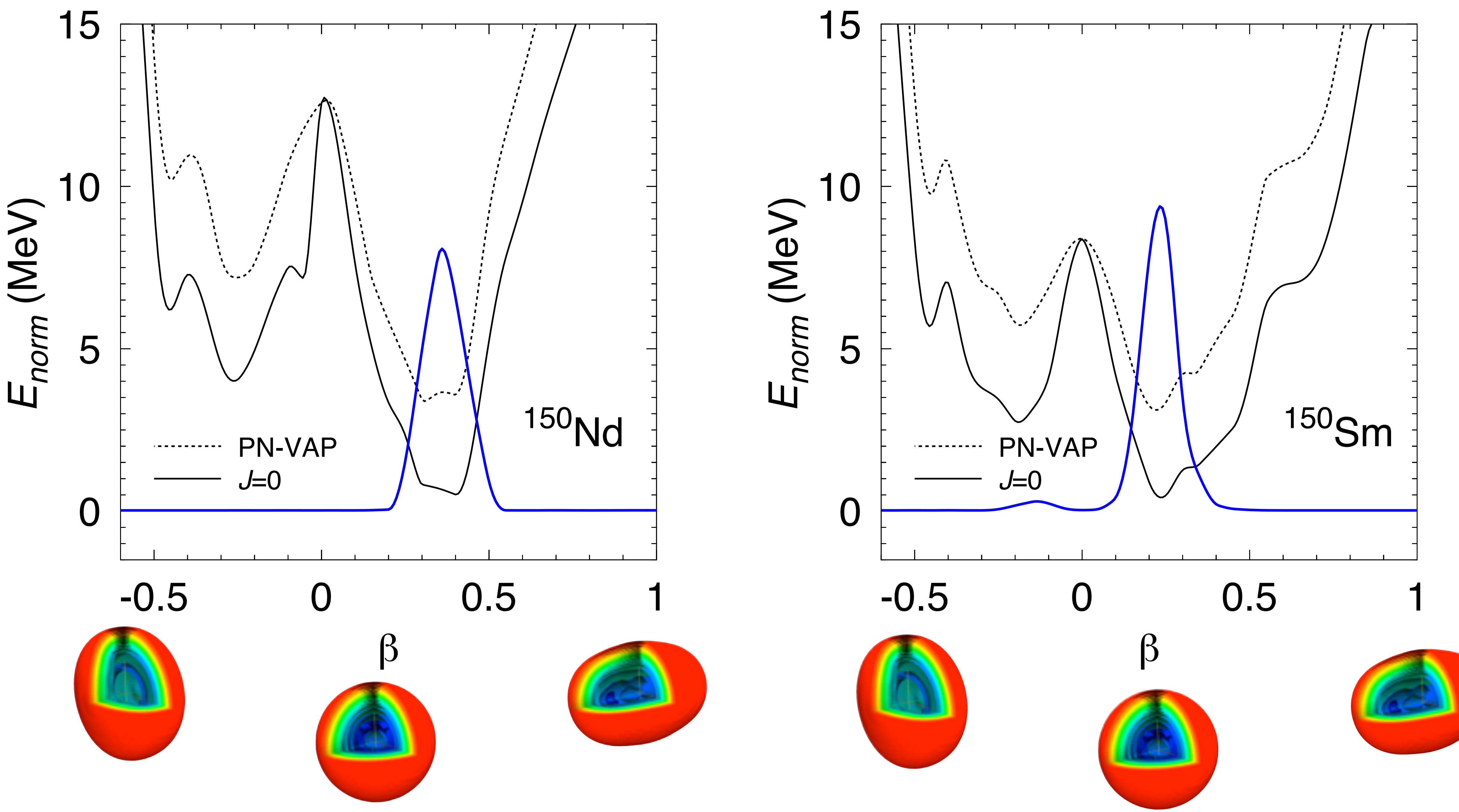

Transitions

UNIVERSIDAD AUTONOMA DE MADRID

1. Axial states $K=0$
2. Angular momentum $I=0$
3. Quadrupole deformations $q=q_{20}$
4. Recently: pairing fluctuations $q=(q_{20},\delta)$

$$\longrightarrow$$

$$|0;N_iZ_i;\sigma\rangle = \sum_{\Lambda_i} G_{\Lambda_i}^{0;N_iZ_i;\sigma}|\Lambda_i^{0;N_iZ_i}\rangle$$

$$|0;N_fZ_f;\sigma\rangle = \sum_{\Lambda_f} G_{\Lambda_f}^{0;N_fZ_f;\sigma}|\Lambda_f^{0;N_fZ_f}\rangle$$

TRANSITIONS:

$$M_\xi^{0\nu\beta\beta} = \langle 0_f^+|\hat{O}_\xi^{0\nu\beta\beta}|0_i^+\rangle = \langle 0;N_fZ_f|\hat{O}_\xi^{0\nu\beta\beta}|0;N_iZ_i\rangle =$$

$$\sum_{\Lambda_f\Lambda_i}\left(G_{\Lambda_f}^{0;N_fZ_f}\right)^*\langle\Lambda_f^{0;N_fZ_f}|\hat{O}_\xi^{0\nu\beta\beta}|\Lambda_i^{0;N_iZ_i}\rangle G_{\Lambda_i}^{0;N_iZ_i} = \sum_{q_iq_f;\Lambda_f\Lambda_i}$$

$$\left(\frac{u_{q_f,\Lambda_f}^{0;N_fZ_f}}{\sqrt{n_{\Lambda_f}^{0;N_fZ_f}}}\right)^*\left(G_{\Lambda_f}^{0;N_fZ_f}\right)^*\langle 0;N_fZ_f;q_f|\hat{O}_\xi^{0\nu\beta\beta}|0;N_iZ_i;q_i\rangle\left(G_{\Lambda_i}^{0;N_iZ_i}\right)\left(\frac{u_{q_i,\Lambda_i}^{0;N_iZ_i}}{\sqrt{n_{\Lambda_i}^{0;N_iZ_i}}}\right)$$

Matrix elements of the double beta transition operators between particle number and angular momentum projected states

Ground state properties

Neutrinoless double beta decay candidates

440 T.R. Rodríguez, G. Martinez-Pinedo / Progress in Particle and Nuclear Physics 66 (2011) 436–440

Table 1
Masses, rms charge radii and total Gamow–Teller strengths $S_{-(+)}$ for mother (granddaughter) calculated with Gogny D1S GCM+PNAMP functional compared to experimental values. Theoretical values for $S_{+/-}$ are quenched by a factor $(0.74)^2$.

Isotope	BEth (MeV)	BE^{exp} (MeV) [27]	Rth (fm)	R^{exp}(fm) [28]	$S^{\mathrm{theo}}_{-/+}$	$S^{\mathrm{exp}}_{-/+}$
^{48}Ca	420.623	415.991	3.465	3.473	13.55	(14.4 ± 2.2 [29])
^{48}Ti	423.597	418.699	3.557	3.591	1.99	(1.9 ± 0.5 [29])
^{76}Ge	664.204	661.598	4.024	4.081	20.97	(19.89 [30])
^{76}Se	664.949	662.072	4.074	4.139	1.49	(1.45 ± 0.07 [31])
^{82}Se	716.794	712.842	4.100	4.139	23.56	(21.91 [30])
^{82}Kr	717.859	714.273	4.130	4.192	1.24	
^{96}Zr	829.432	828.995	4.298	4.349	27.63	
^{96}Mo	833.793	830.778	4.319	4.384	2.56	(0.29 ± 0.08 [32])
^{100}Mo	861.526	860.457	4.372	4.445	27.87	(26.69 [30])
^{100}Ru	864.875	861.927	4.388	4.453	2.48	
^{116}Cd	988.469	987.440	4.556	4.628	34.30	(32.70 [30])
^{116}Sn	991.079	988.684	4.567	4.626	2.61	($1.09^{+0.13}_{-0.57}$ [33])
^{124}Sn	1051.668	1049.96	4.622	4.675	40.65	
^{124}Te	1051.562	1050.69	4.664	4.717	1.63	
^{128}Te	1082.257	1081.44	4.686	4.735	40.48	(40.08 [30])
^{128}Xe	1080.996	1080.74	4.723	4.775	1.45	
^{130}Te	1096.627	1095.94	4.695	4.742	43.57	(45.90 [30])
^{130}Xe	1097.245	1096.91	4.732	4.783	1.19	
^{136}Xe	1143.333	1141.88	4.756	4.799	46.71	
^{136}Ba	1143.202	1142.77	4.786	4.832	0.96	
^{150}Nd	1234.512	1237.45	5.034	5.041	50.32	
^{150}Sm	1235.936	1239.25	5.041	5.040	1.45	

Good agreement between experimental and theoretical Q-values, radii and total strength (quenched)

NME: deformation and mixing

T.R.R., Martínez-Pinedo, PRL 105, 252503 (2010)

$$\frac{\langle 0; N_f Z_f; q_f | \hat{O}_{\xi}^{0\nu\beta\beta} | 0; N_i Z_i; q_i \rangle}{\sqrt{\langle 0; N_f Z_f; q_f | 0; N_f Z_f; q_f \rangle \langle 0; N_i Z_i; q_i | 0; N_i Z_i; q_i \rangle}}$$

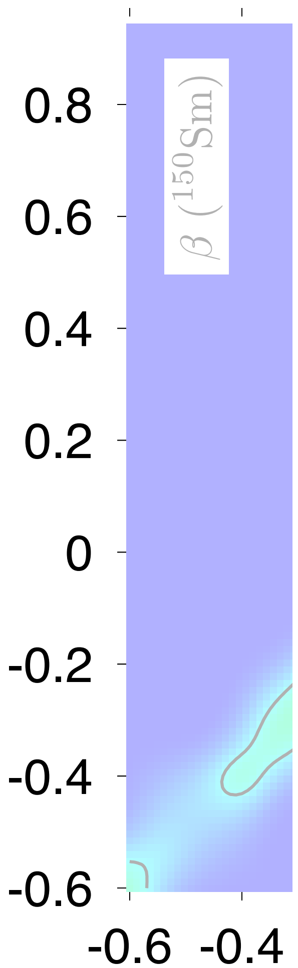

A=150

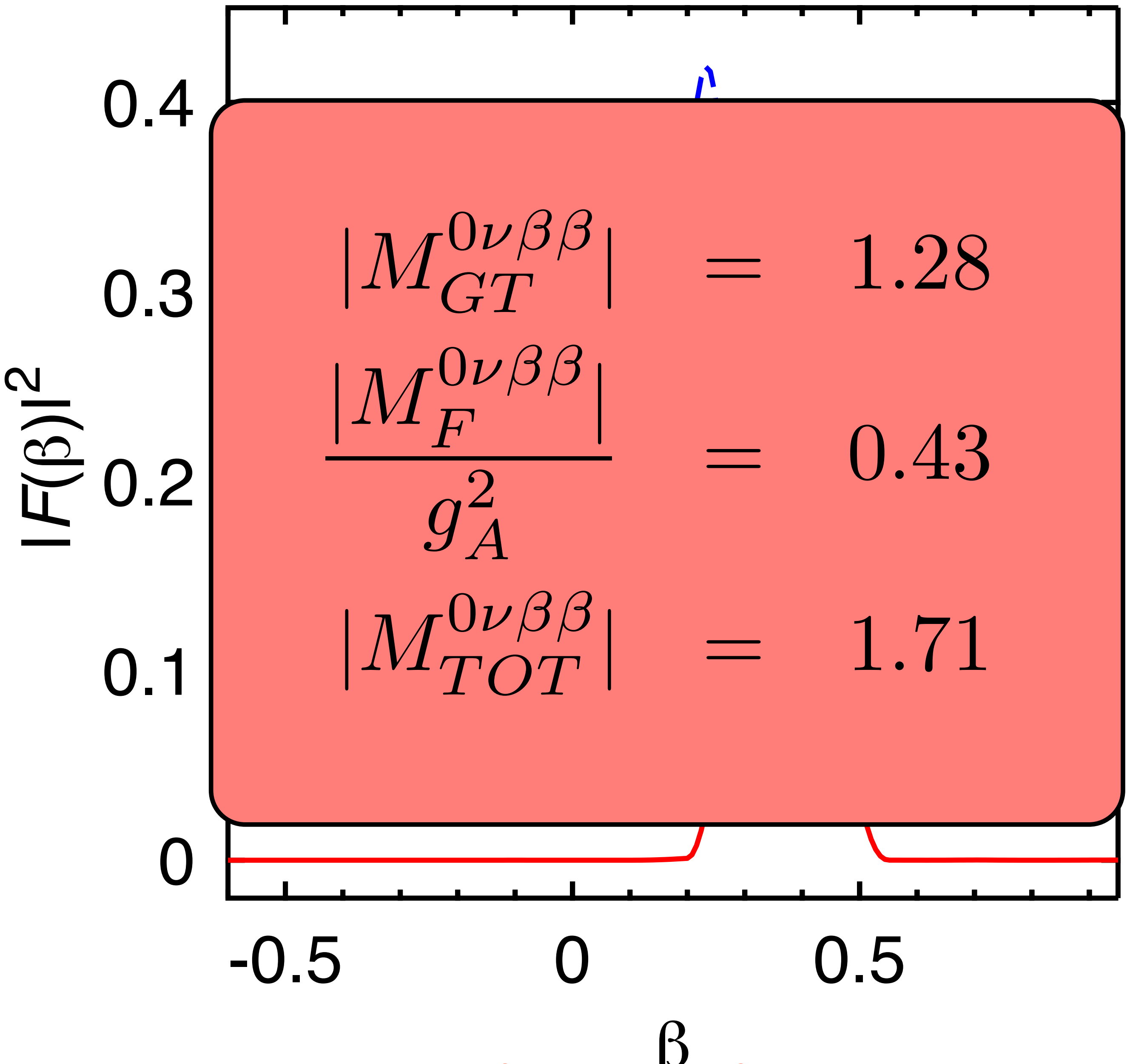

$$|M_{GT}^{0\nu\beta\beta}| = 1.28$$

$$\frac{|M_{F}^{0\nu\beta\beta}|}{g_A^2} = 0.43$$

$$|M_{TOT}^{0\nu\beta\beta}| = 1.71$$

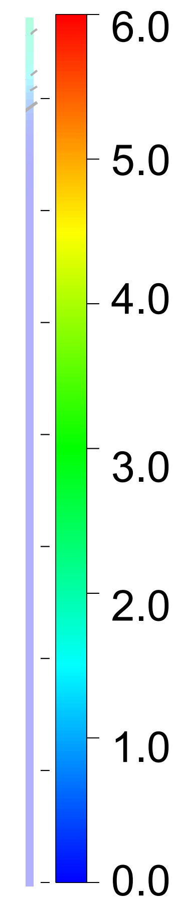

- GT streng
- Similar de
- Maxima a
- Final result depends on the distribution of probability of the corresponding initial and final collective states within this plot

NME: deformation and mixing

$$\frac{\langle 0; N_f Z_f; q_f | \hat{O}_{\xi}^{0\nu\beta\beta} | 0; N_i Z_i; q_i \rangle}{\sqrt{\langle 0; N_f Z_f; q_f | 0; N_f Z_f; q_f \rangle \langle 0; N_i Z_i; q_i | 0; N_i Z_i; q_i \rangle}}$$

A=76

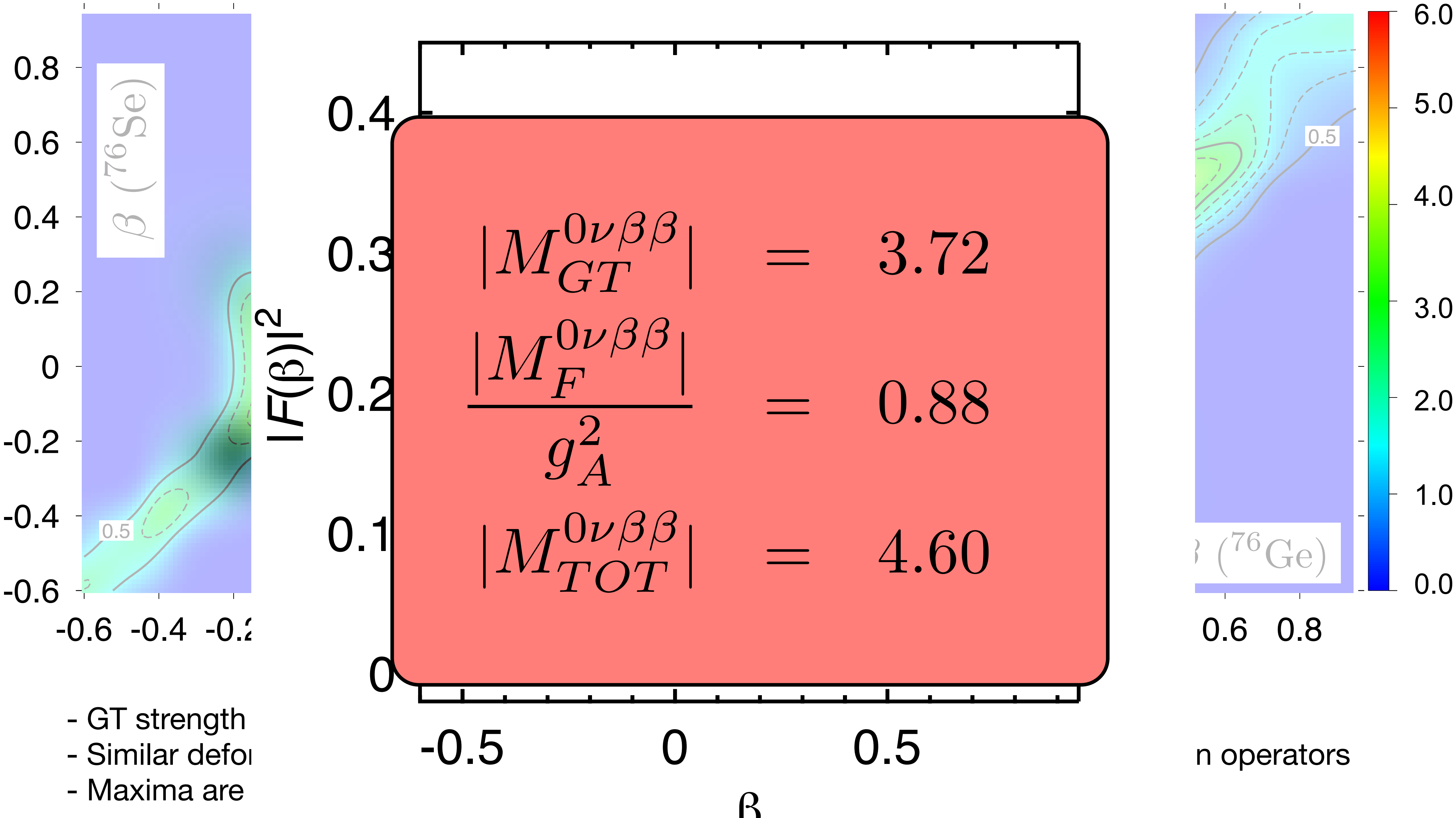

$$|M_{GT}^{0\nu\beta\beta}| = 3.72$$

$$\frac{|M_{F}^{0\nu\beta\beta}|}{g_A^2} = 0.88$$

$$|M_{TOT}^{0\nu\beta\beta}| = 4.60$$

- GT strength
- Similar defo
- Maxima are

n operators

- Final result depends on the distribution of probability of the corresponding initial and final collective states within this plot

Shape and pp/nn pairing fluctuations

Angular momentum projected potential energy surfaces

Collective ground state wave functions

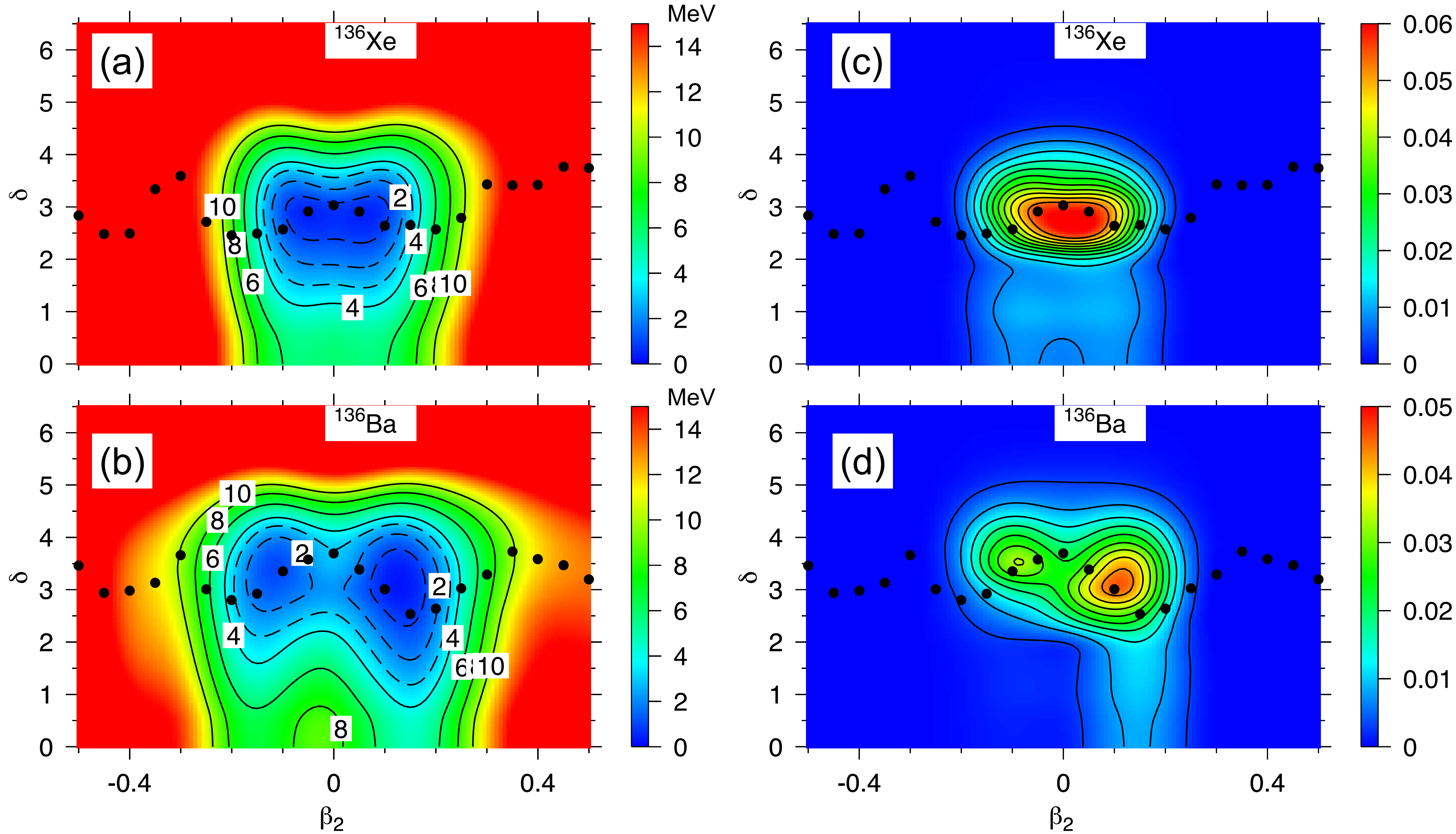

N. López-Vaquero, T.R.R., J.L. Egido, PRL 111, 142501 (2013)

Shape and pp/nn pairing fluctuations

Dependence on deformation

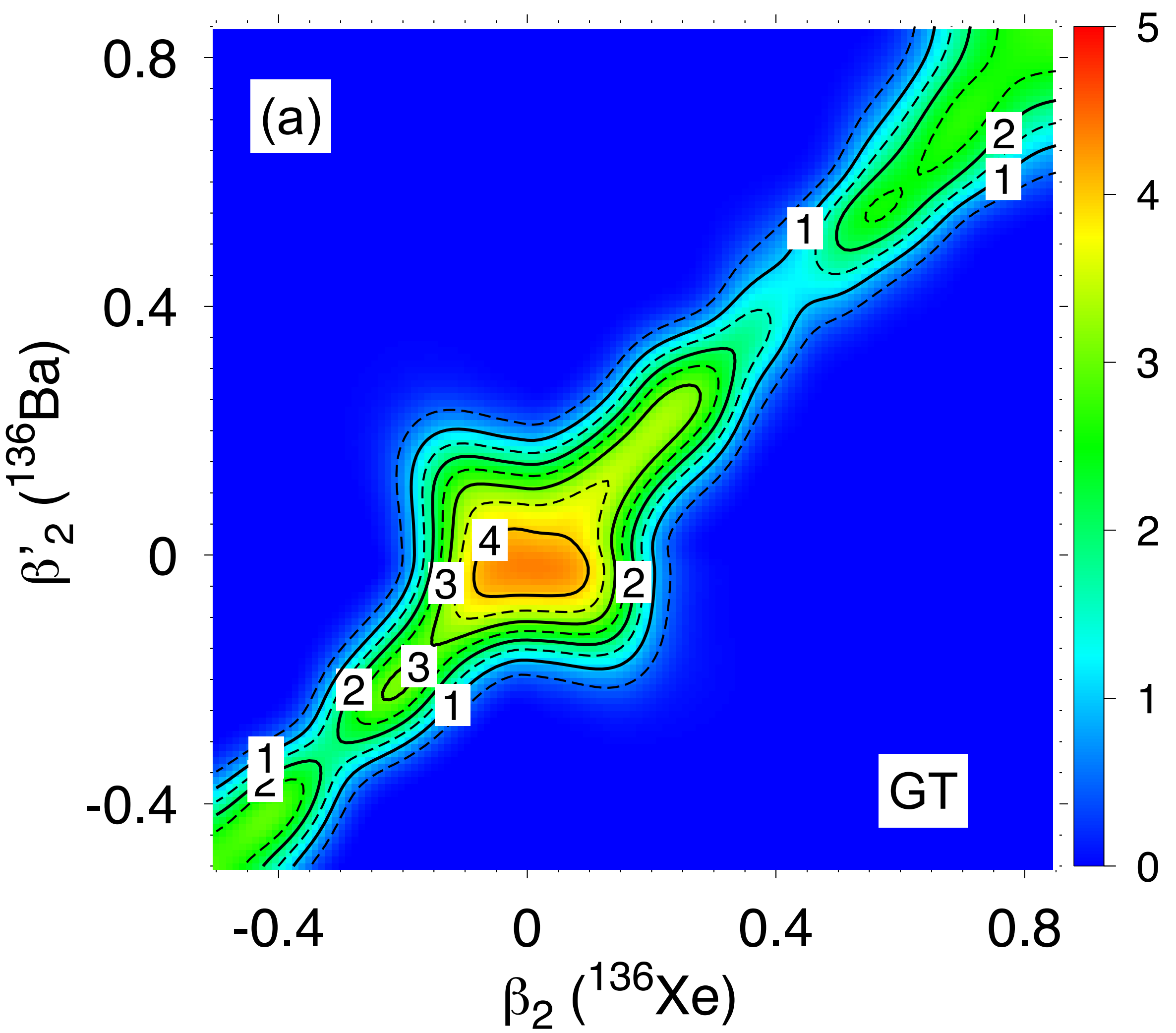

Dependence on pp/nn pairing

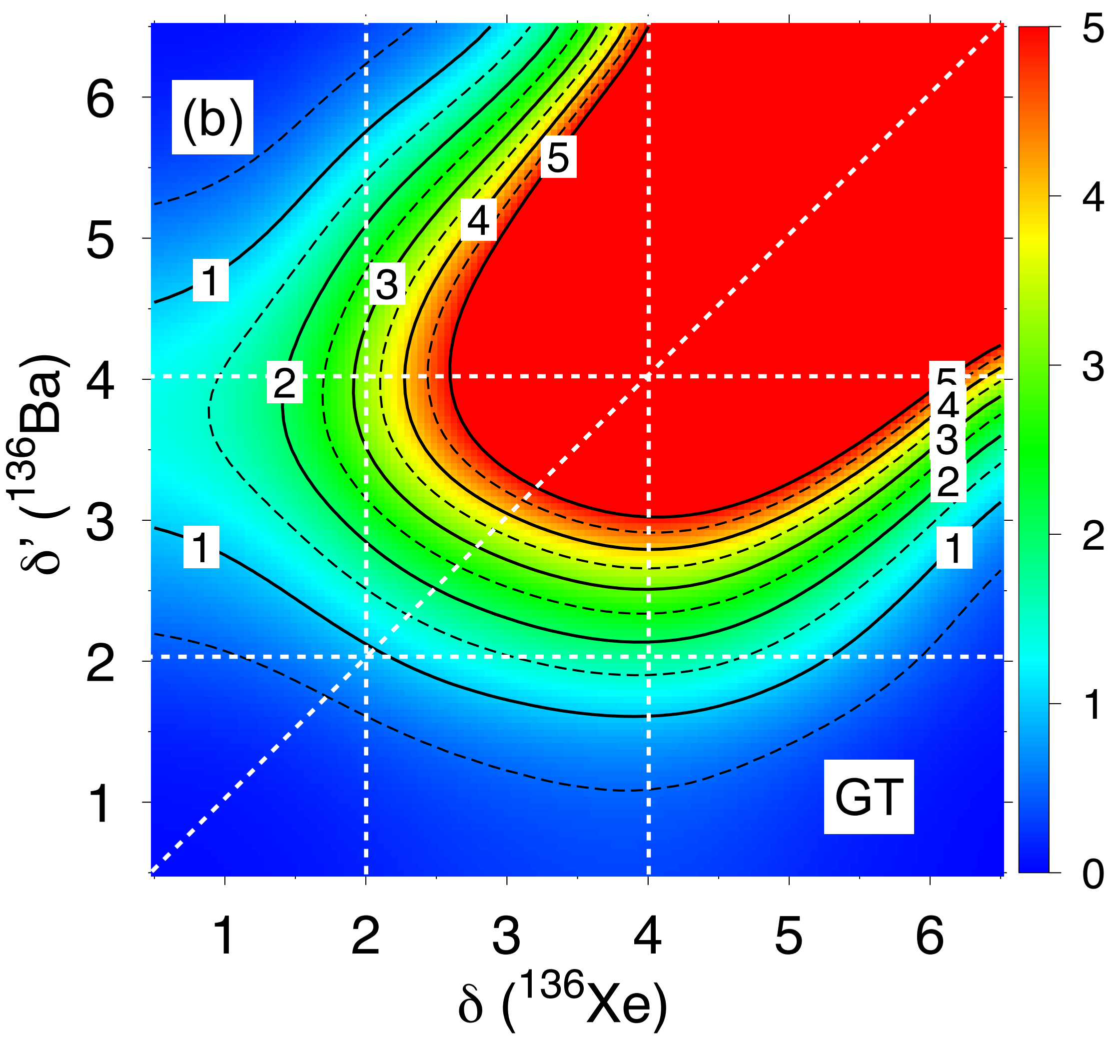

N. López-Vaquero, T.R.R., J.L. Egido, PRL 111, 142501 (2013)

NME: Summary of the results II

Isotope	$\Delta Q(\beta_2)$	$\Delta Q(\beta_2,\delta)$	$M^{0\nu}(\beta_2)$	$M^{0\nu}(\beta_2,\delta)$	Var (%)	$\frac{T_{1/2}(\beta_2,\delta)}{T_{1/2}(\beta_2)}$
^{48}Ca	0.265	0.131	$2.370^{1.914}_{0.456}$	$2.229^{1.797}_{0.431}$	-6	1.13
^{76}Ge	0.271	0.190	$4.601^{3.715}_{0.886}$	$5.551^{4.470}_{1.082}$	21	0.69
^{82}Se	-0.366	-0.246	$4.218^{3.381}_{0.837}$	$4.674^{3.743}_{0.931}$	11	0.81
^{96}Zr	2.580	2.628	$5.650^{4.618}_{1.032}$	$6.498^{5.296}_{1.202}$	15	0.76
^{100}Mo	1.879	1.757	$5.084^{4.149}_{0.935}$	$6.588^{5.361}_{1.227}$	30	0.60
^{116}Cd	1.365	1.337	$4.795^{3.931}_{0.864}$	$5.348^{4.372}_{0.976}$	12	0.80
^{124}Sn	-0.830	-0.687	$4.808^{3.893}_{0.916}$	$5.787^{4.680}_{1.107}$	20	0.69
^{128}Te	-0.564	-0.594	$4.107^{3.079}_{1.027}$	$5.687^{4.255}_{1.432}$	38	0.52
^{130}Te	-0.348	-0.628	$5.130^{4.141}_{0.989}$	$6.405^{5.161}_{1.244}$	25	0.64
^{136}Xe	-1.027	-0.787	$4.199^{3.673}_{0.526}$	$4.773^{4.170}_{0.604}$	14	0.77
^{150}Nd	-0.380	-0.282	$1.707^{1.278}_{0.429}$	$2.190^{1.639}_{0.551}$	29	0.61

N. López-Vaquero, T.R.R., J.L. Egido, PRL 111, 142501 (2013)

pn pairing fluctuations

$$H = h_0 - \sum_{\mu=-1}^{1} g_{\mu}^{T=1}\, S_{\mu}^{\dagger} S_{\mu} - \frac{\chi}{2} \sum_{K=-2}^{2} Q_{2K}^{\dagger} Q_{2K}$$

$$- g^{T=0} \sum_{\nu=-1}^{1} P_{\nu}^{\dagger} P_{\nu} + \ldots$$

where h_0 contains spherical ... are the components of a qu... Ref. [15], and

$$S_{\mu}^{\dagger} = \frac{1}{\sqrt{2}} \sum_l \hat{l}[c_l^{\dagger} c_l^{\dagger}]_{00\mu}^{001}\,, \ldots$$

$$F_{\nu}^{\mu} = \frac{1}{2} \sum_i \sigma_i^{\mu} \tau_i^{\nu} = \sum_l \hat{l}[c_l^{\dagger} \bar{c}_l]_{0\mu\nu}^{011}\,. \qquad (3)$$

$$H' = H - \lambda_Z N_Z - \lambda_N N_N - \lambda_Q Q_{20} - \frac{\lambda_P}{2}\left(P_0 + P_0^{\dagger}\right)\,, \quad (6)$$

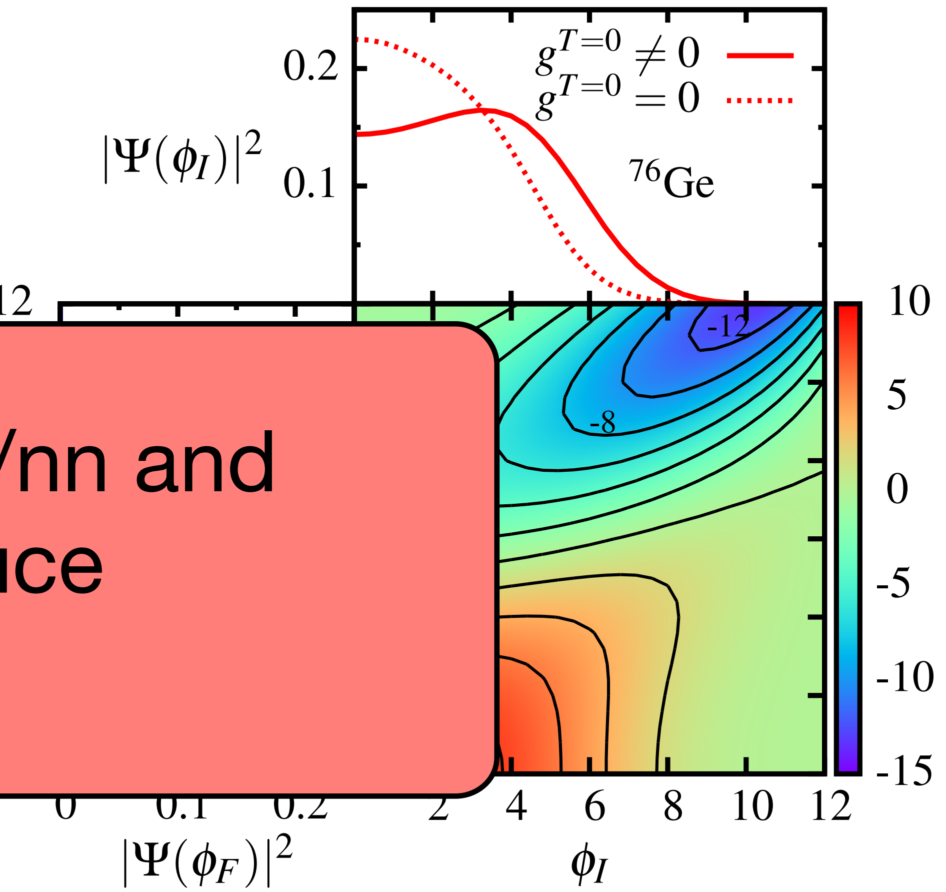

FIG. 3. (Color online.) **Bottom right:** $\mathcal{N}_{\phi_I}\mathcal{N}_{\phi_F}\langle\phi_F|\mathcal{P}_F \hat{M}_{0\nu}\mathcal{P}_I|\phi_I\rangle$ for projected quasiparticle vacua with different values of the initial and final isoscalar pairing amplitudes ϕ_I and ϕ_F, from the SkO′-based interaction (see text). **Top and bottom left:** Square of collective wave functions in ^{76}Ge and ^{76}Se.

Exploring explicitly pp/nn and pn pairing could produce cancellations

N. Hinohara and J. Engel, PRC 031031(R) (2014)

NME: $^{116}Cd \rightarrow {}^{116}Sn$

A=116 (possible candidate for detection)

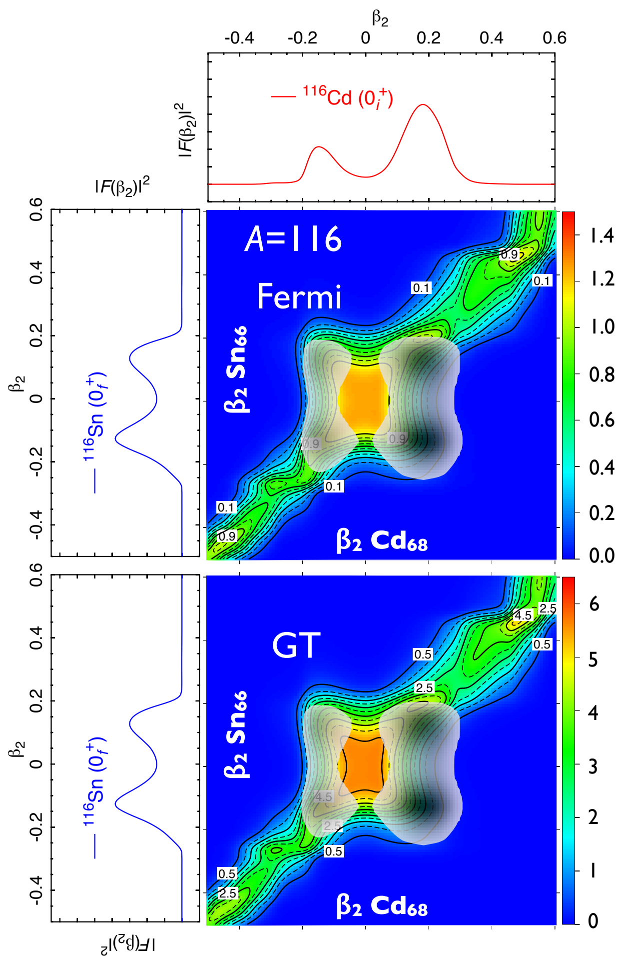

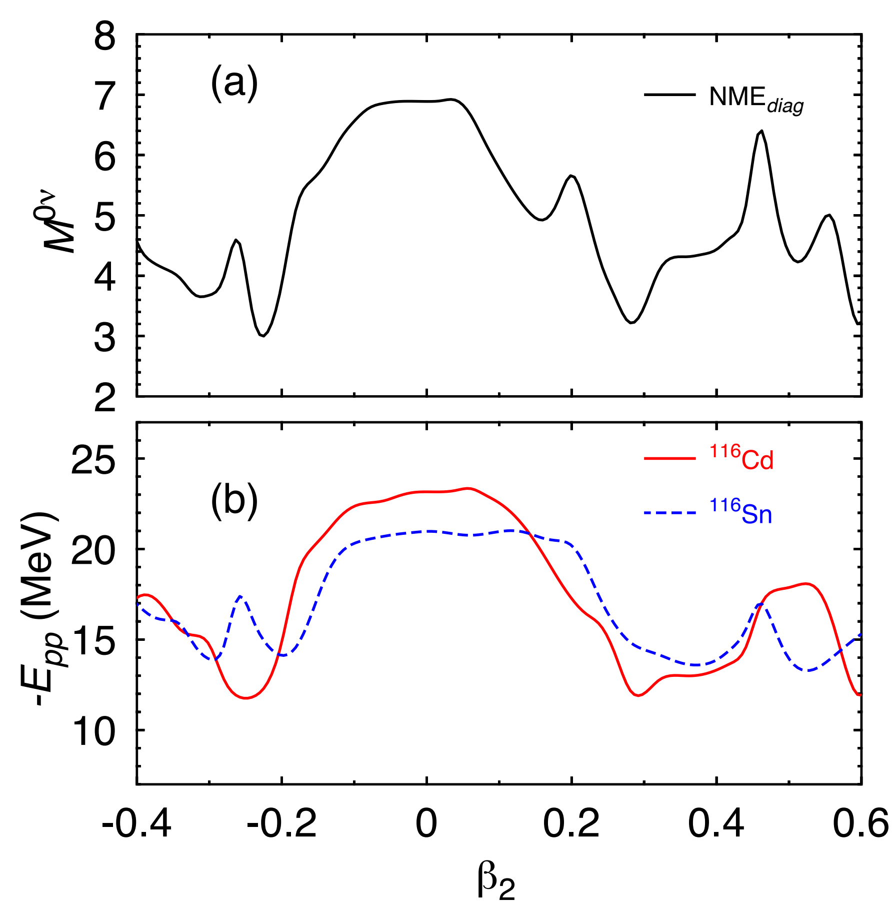

- Reduction of the NME with respect to the spherical value when shape mixing is included

- Larger pairing correlations in mother/ daughter nuclei produces larger NMEs.

NME: ^{A}Cd→^{A}Sn Shell Effects

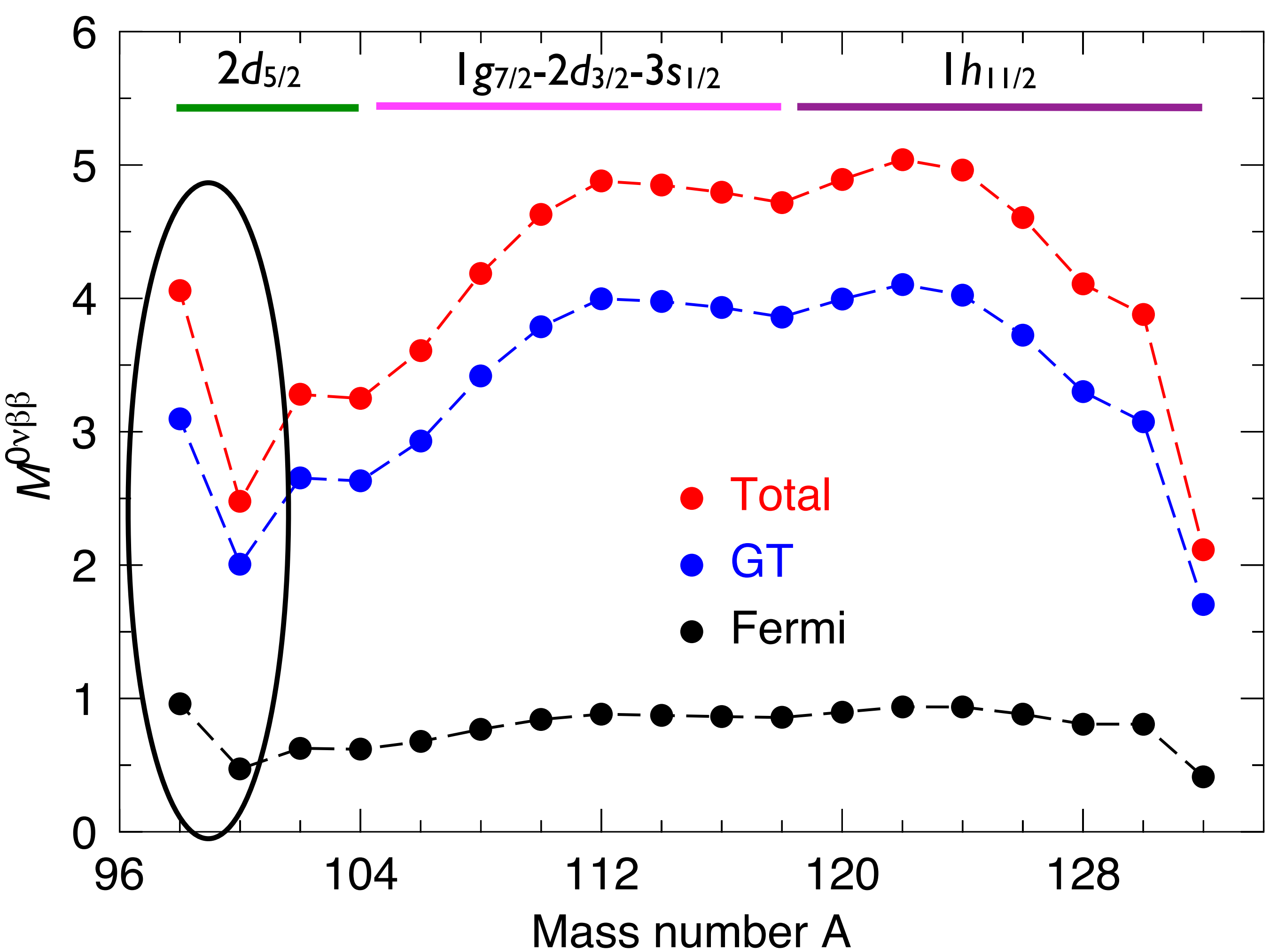

T.R.R., Martínez-Pinedo, PLB 719, 174 (2013)

- GT component is always larger than Fermi.
- Large enhancement of the NME for the mirror decay A=98.
- Shell effects associated to the filling of neutrons in the corresponding sub-shells. Consistent with seniority model.

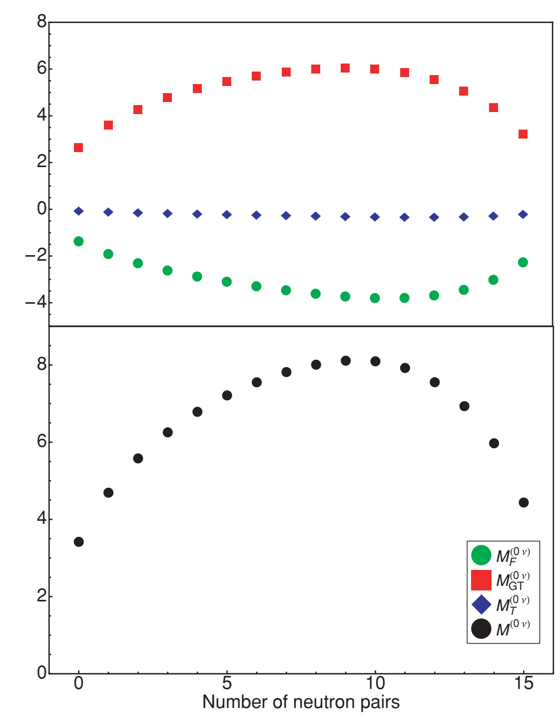

J. Barea and F. Iachello, Phys. Rev. C 79, 044301 (2009)

NME: ^{A}Cd→^{A}Sn

UNIVERSIDAD AUTONOMA DE MADRID

- Reduction of the NME with respect to the spherical value when shape mixing is included
- Larger reduction when the difference in deformation is larger

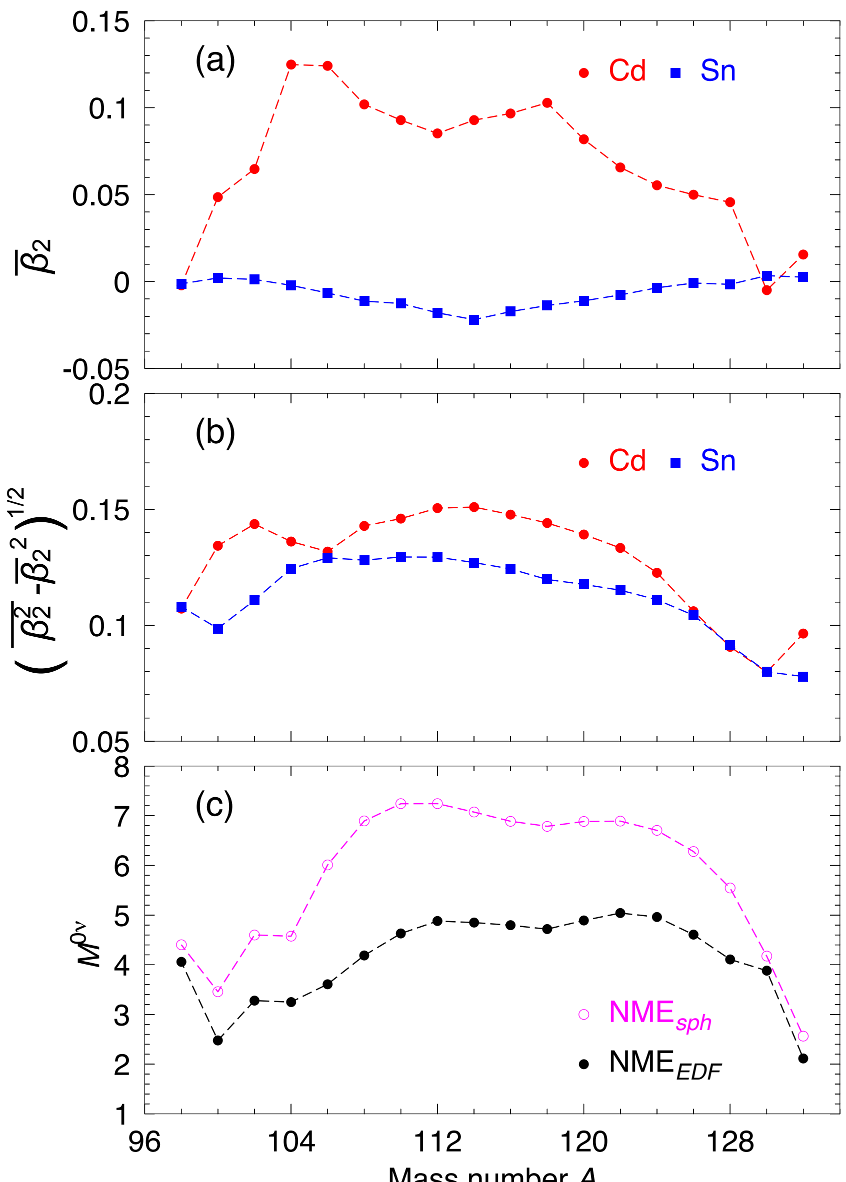

- Larger pairing correlations in mother/daughter nuclei produces larger NMEs.

- Closely related to shell effects

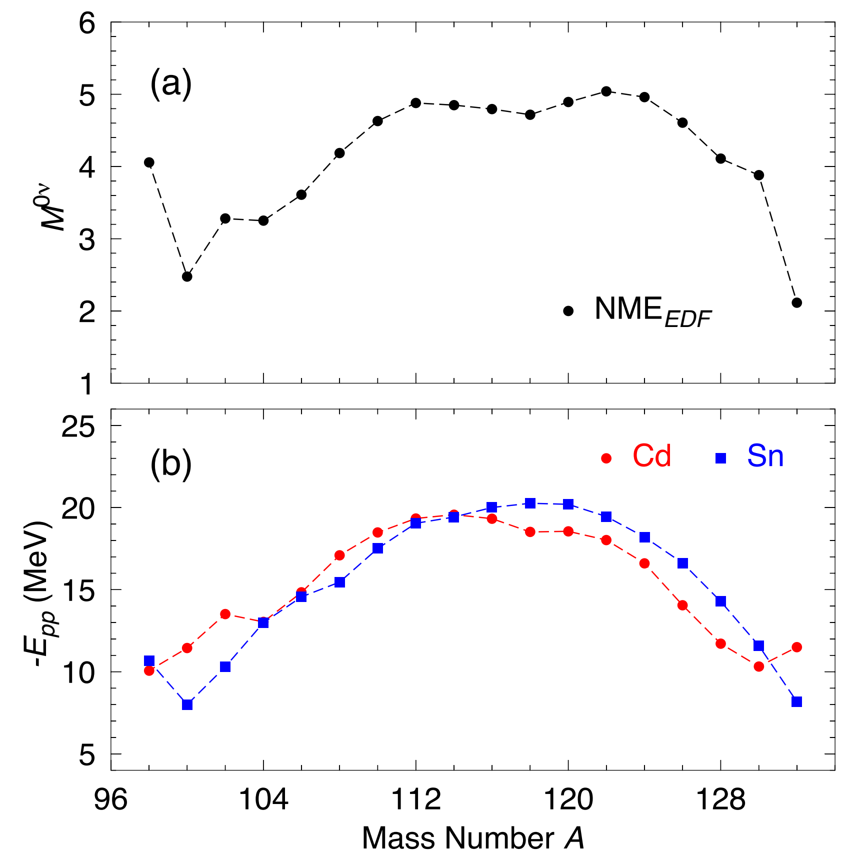

T.R.R., Martínez-Pinedo, PLB 719, 174 (2013)

NME: *pf*-shell

Where do the differences come from?

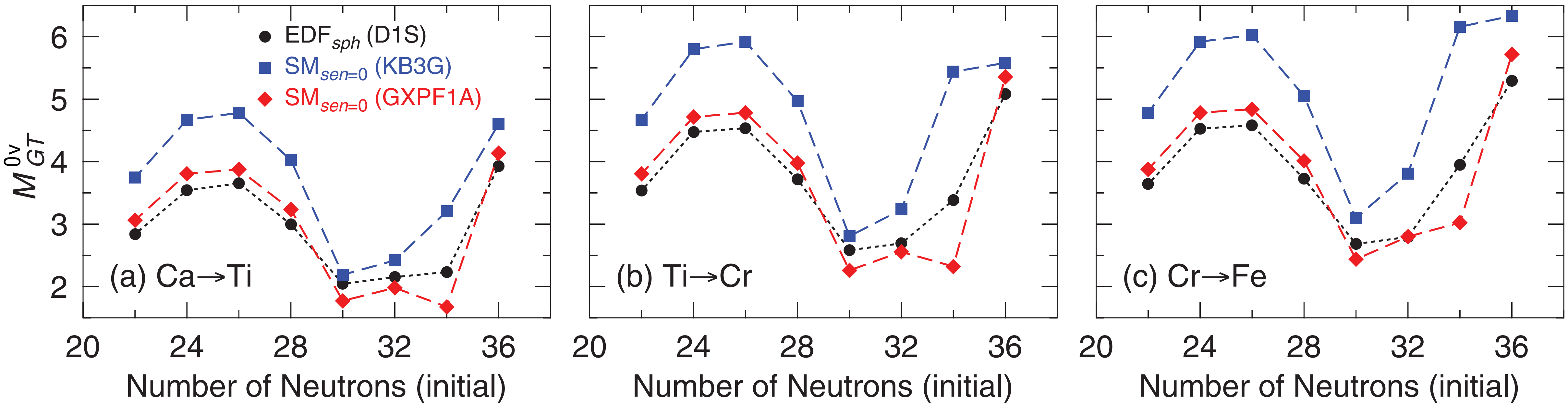

- Same pattern in spherical EDF, seniority 0 Shell Model, and Generalized Seniority model (overall scale?)

- What is the effect of including more **correlations**?

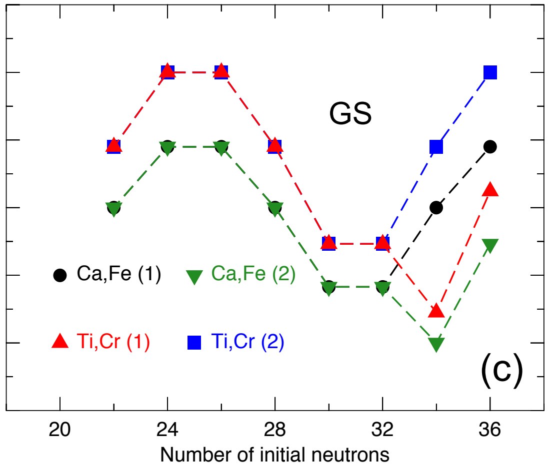

J. Menéndez, T. R. R., A. Poves, G. Martínez-Pinedo, PRC 90, 024311 (2014).

NME: *pf*-shell

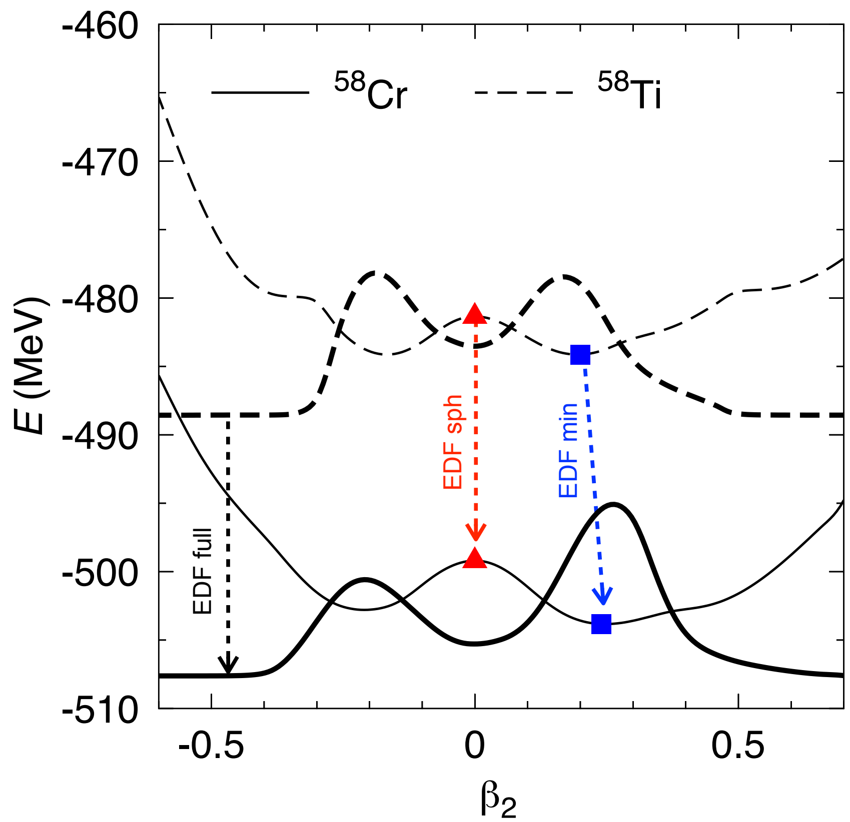

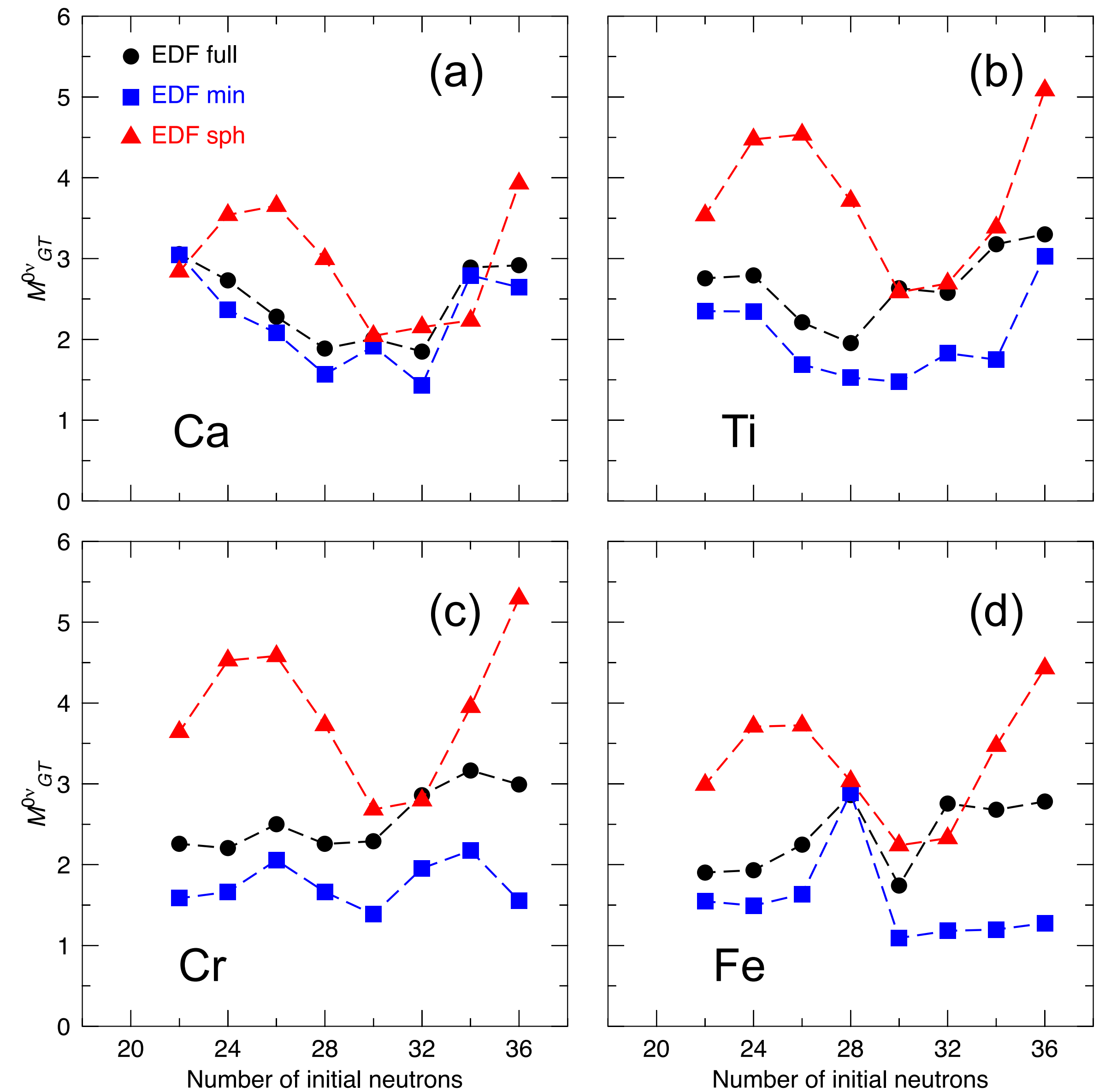

- NMEs are reduced with respect to the spherical value when correlations are included.

- The biggest reduction is produced by angular momentum restoration and configuration mixing produces an increase of the NME.

- Cross-check nuclei: ^{42}Ca, ^{50}Ca, ^{56}Fe

J. Menéndez, T. R. R., A. Poves, G. Martínez-Pinedo, PRC 90, 024311 (2014).

NME: *pf*-shell

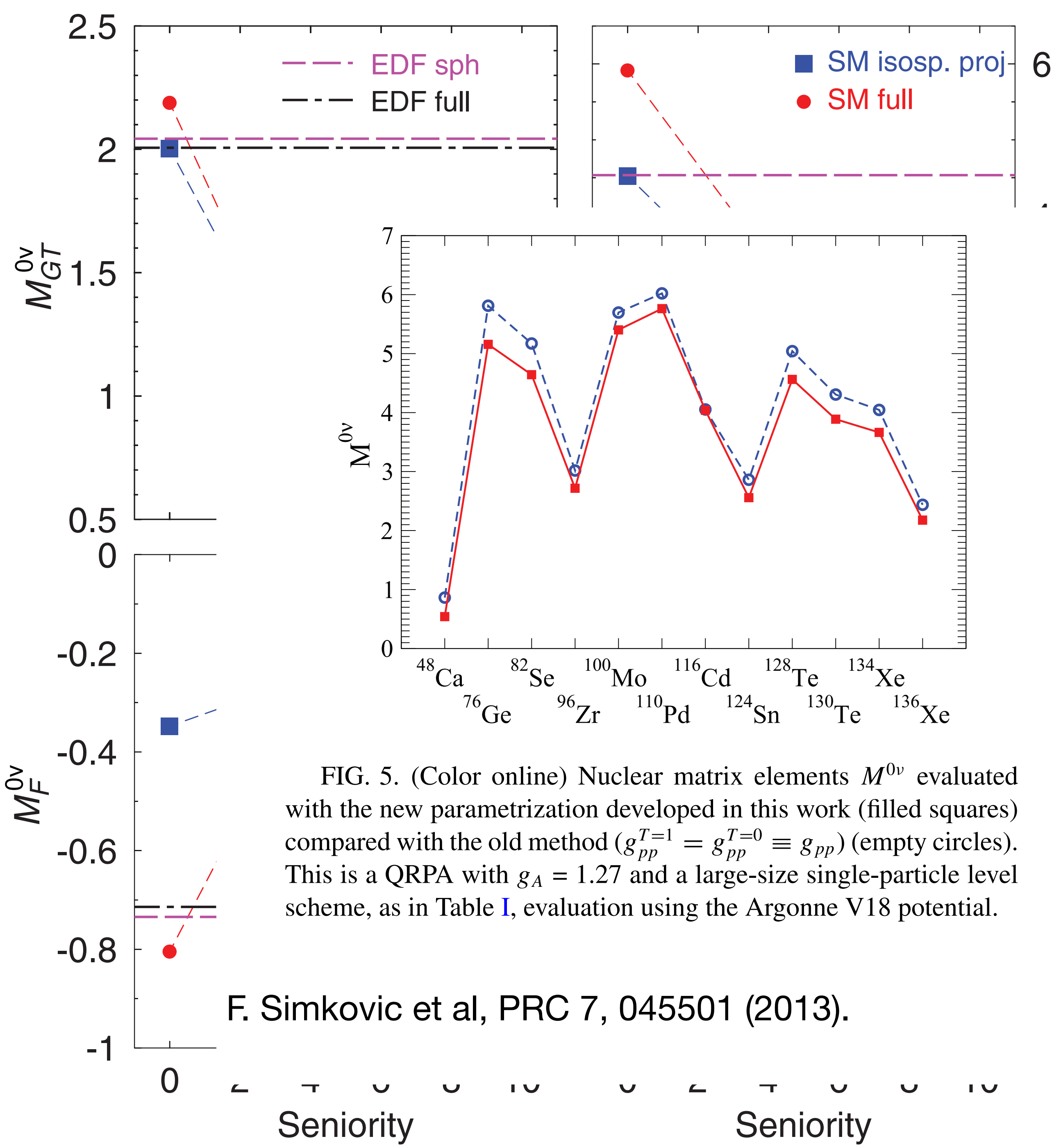

FIG. 5. (Color online) Nuclear matrix elements $M^{0\nu}$ evaluated with the new parametrization developed in this work (filled squares) compared with the old method ($g_{pp}^{T=1} = g_{pp}^{T=0} \equiv g_{pp}$) (empty circles). This is a QRPA with $g_A = 1.27$ and a large-size single-particle level scheme, as in Table I, evaluation using the Argonne V18 potential.

F. Simkovic et al, PRC 7, 045501 (2013).

- The biggest reduction (in Shell model calculations) is produced by including higher seniority components in the nuclear wave functions.
- Isospin projection is relevant for the Fermi part of the NME and less important for the Gamow-Teller part.
- Isospin projection tends to reduce the NME.
- EDF does not include properly those higher seniority components, specially in spherical nuclei.
- p-n pairing effects could also be important in the reduction of the NME.

J. Menéndez, T. R. R., A. Poves, G. Martínez-Pinedo, PRC 90, 024311 (2014).

Occupation numbers

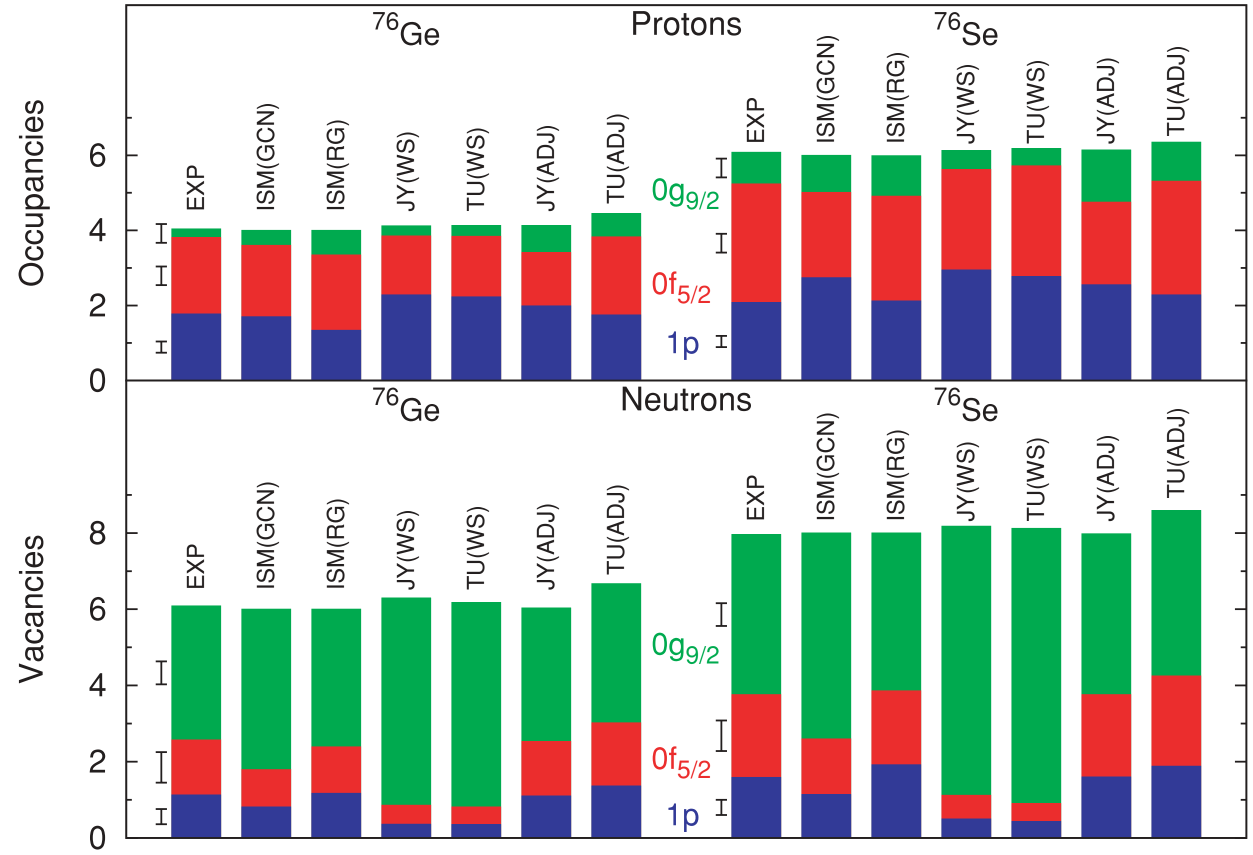

FIG. 1. (Color online) Comparison between experimental and theoretical occupation numbers for $A = 76$. Experimental values are from Refs. [1,2]. The ISM results correspond to the gcn28.50 (GCN) and rg (RG) interactions. The QRPA standard numbers, TU(WS) and JY(WS) give the occupancies at the BCS level. The QRPA occupancies with adjusted single particle energies are given at the BCS level in the case of JY(ADJ) and at QRPA level for TU(ADJ). JY and TU results from Refs. [5] and [6], respectively. The experimental error bars are also shown.

$M^{0\nu\beta\beta}$	GCN	WS	RG	ADJ-WS
ISM	2.81		3.26	
QRPA(JY)		5.36		4.11
QRPA(TU)		5.07–6.25		4.59–5.44

Fitting the underlying (WS) mean field to reproduce the experimental occupation numbers reduces the pnQRPA NMEs.

J. Menéndez et al., Phys. Rev. C 80, 048501 (2009)

Exp: J. Schiffer et al., Phys Rev. Lett. 100, 112501 (2008)

Occupation numbers

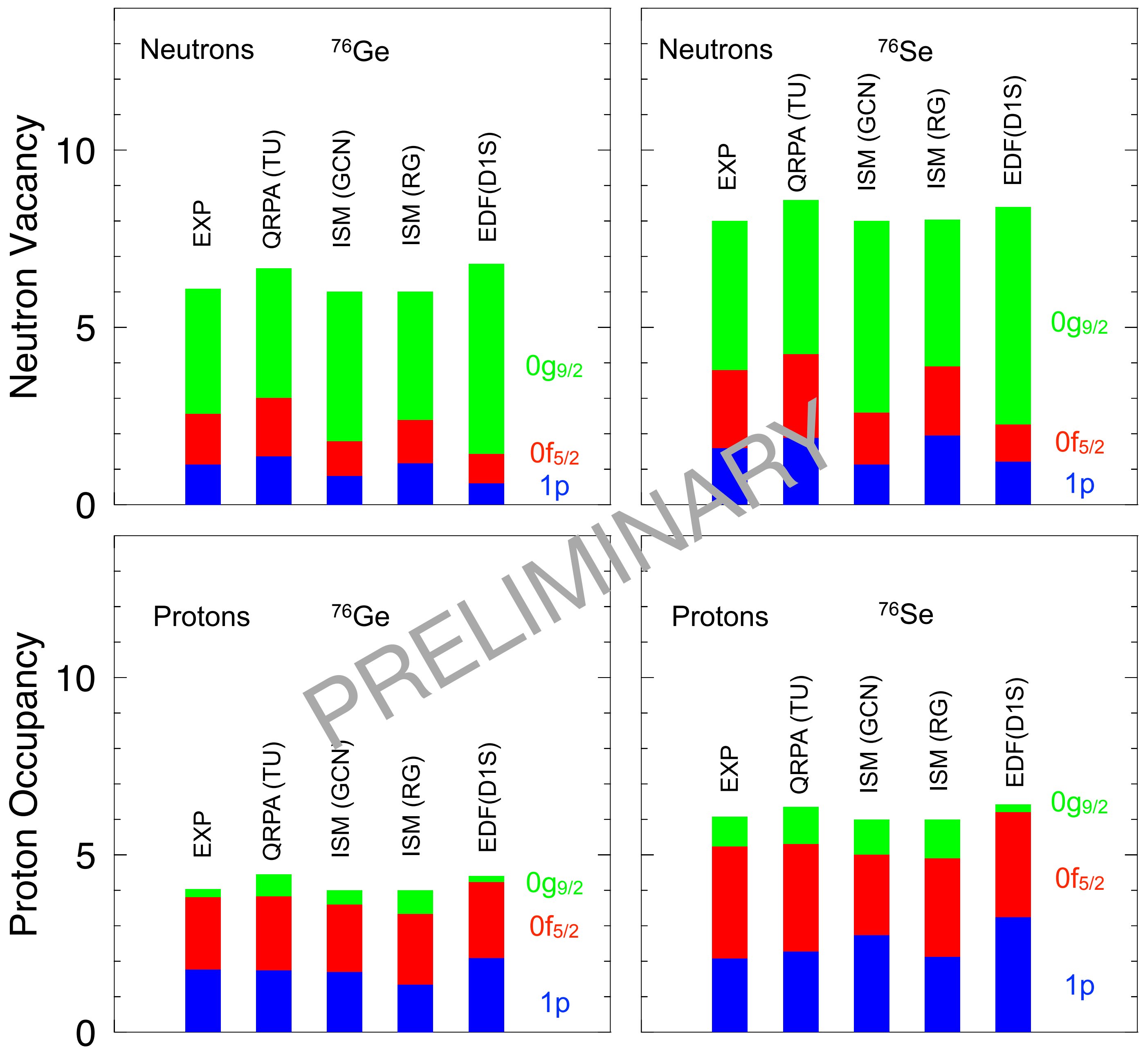

Occupation numbers

✓ The spherical wave function defines the spherical ("shell model like") orbits.

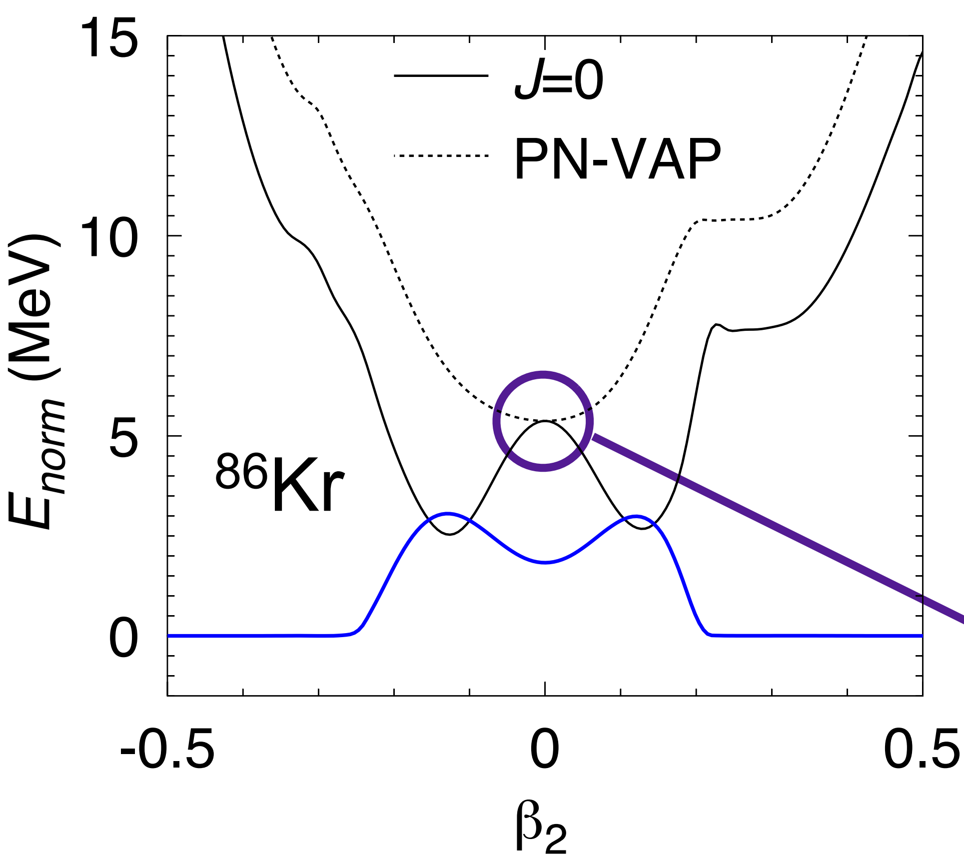

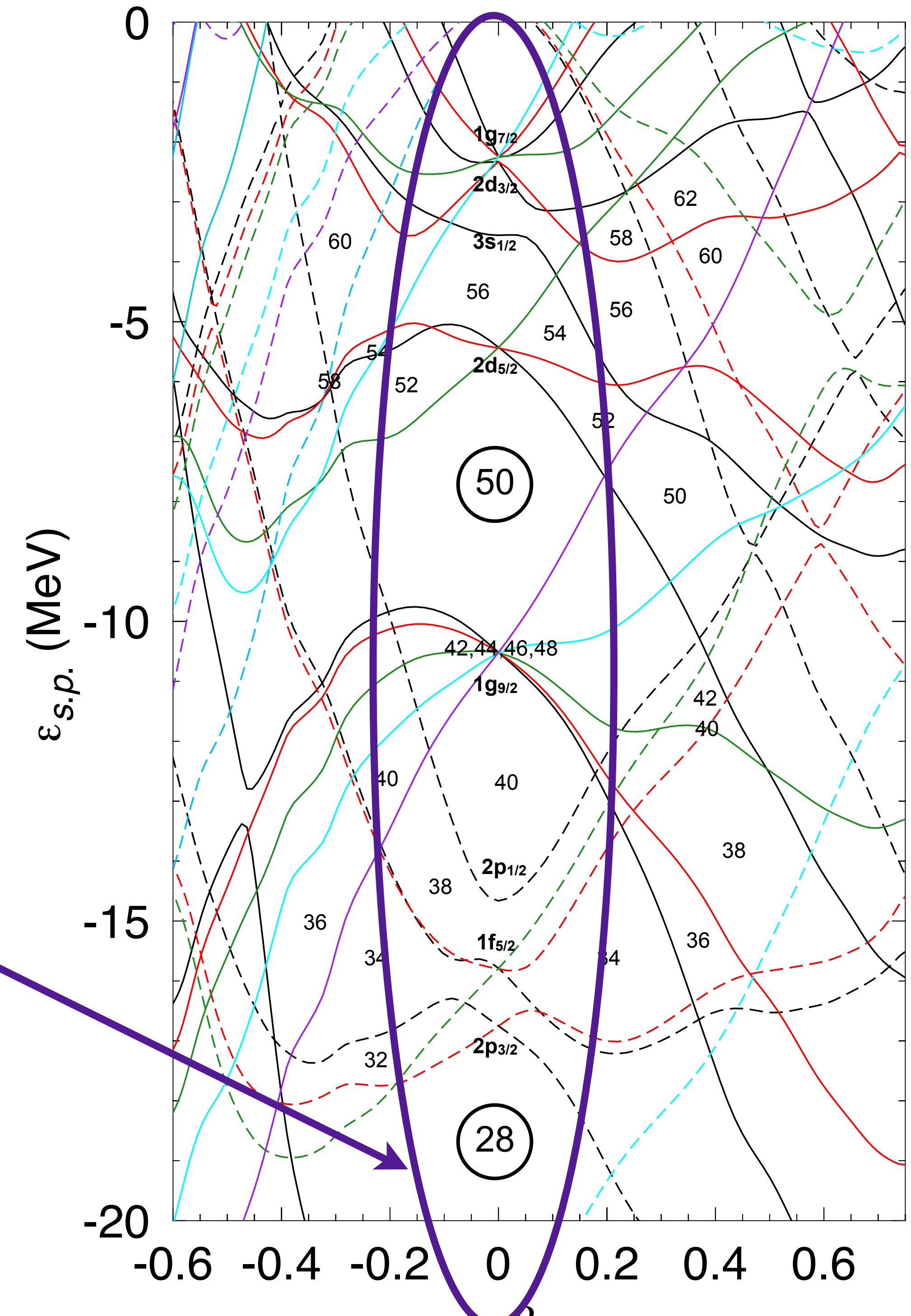

T. R. R., in preparation

Occupation numbers

✓ The spherical wave function defines the spherical ("shell model like") orbits.

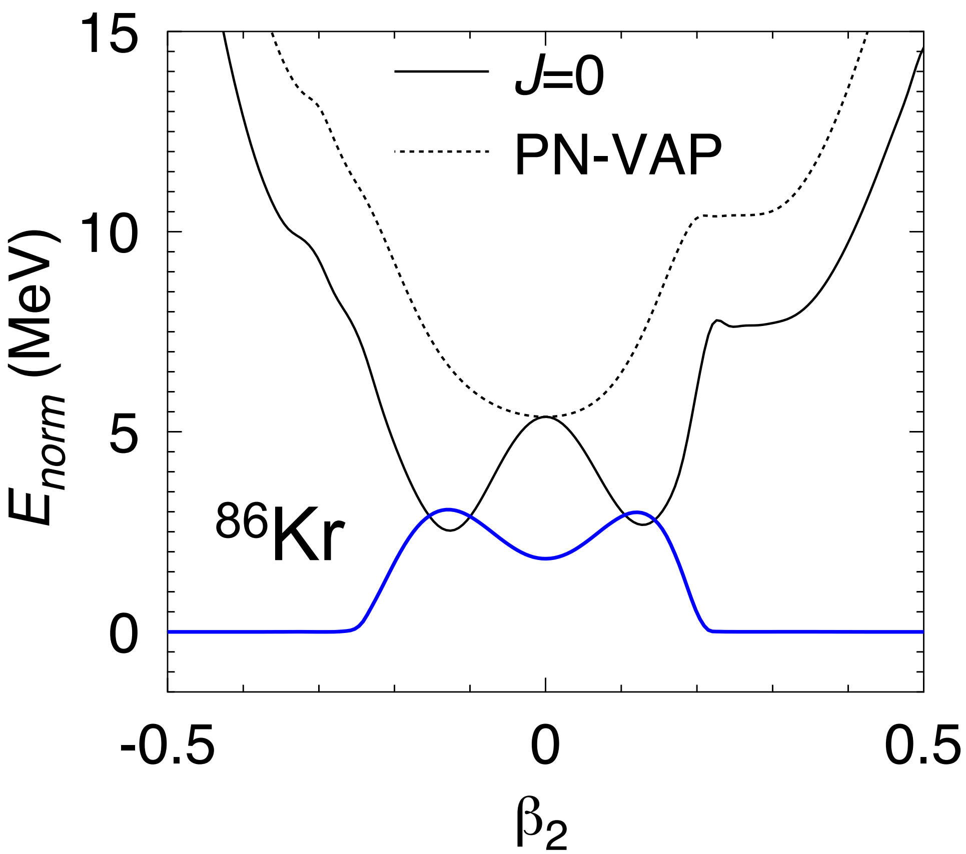

✓ The spherical shells are filled in or emptying depending on the deformation.

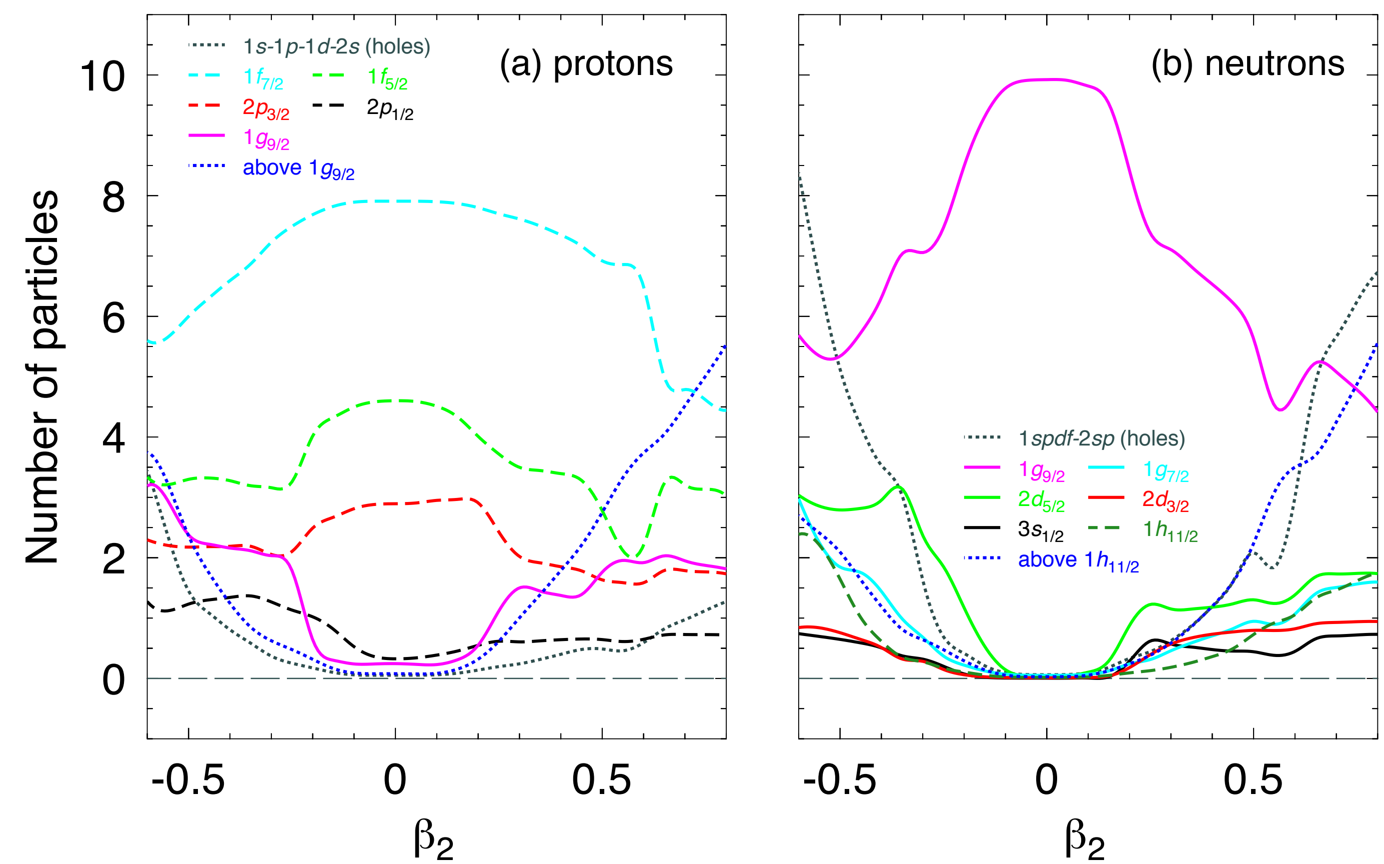

✓ The final occupation of each shell corresponding to a many-body state is computed with the GCM wave functions.

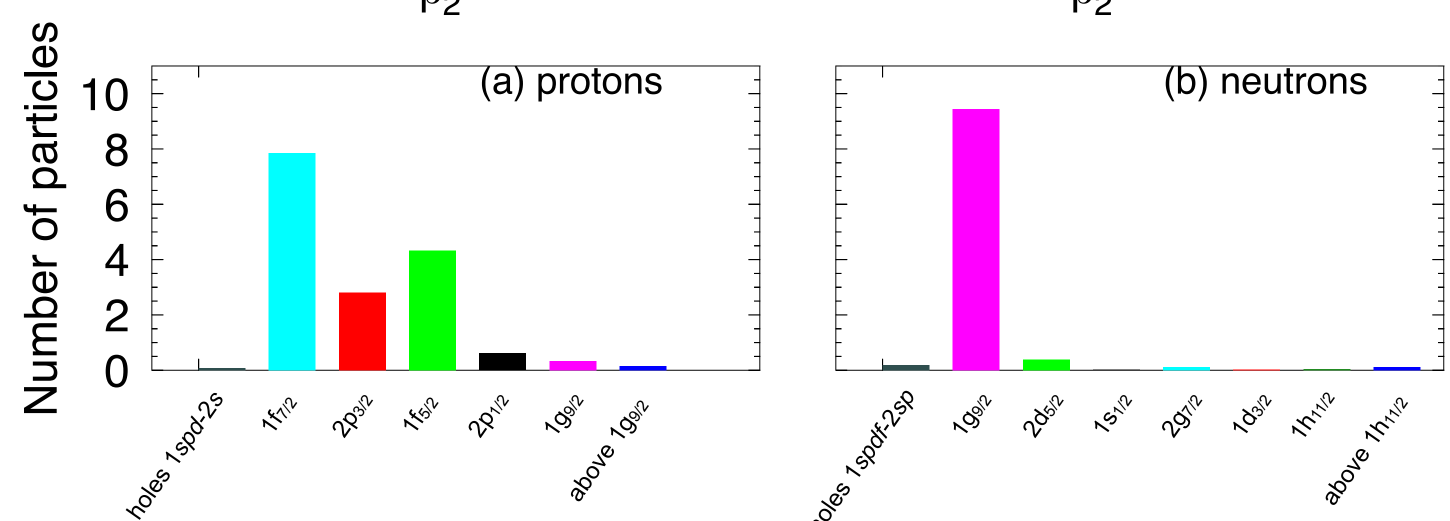

T. R. R., in preparation

Occupation numbers

✓ The spherical wave function defines the spherical ("shell model like") orbits.

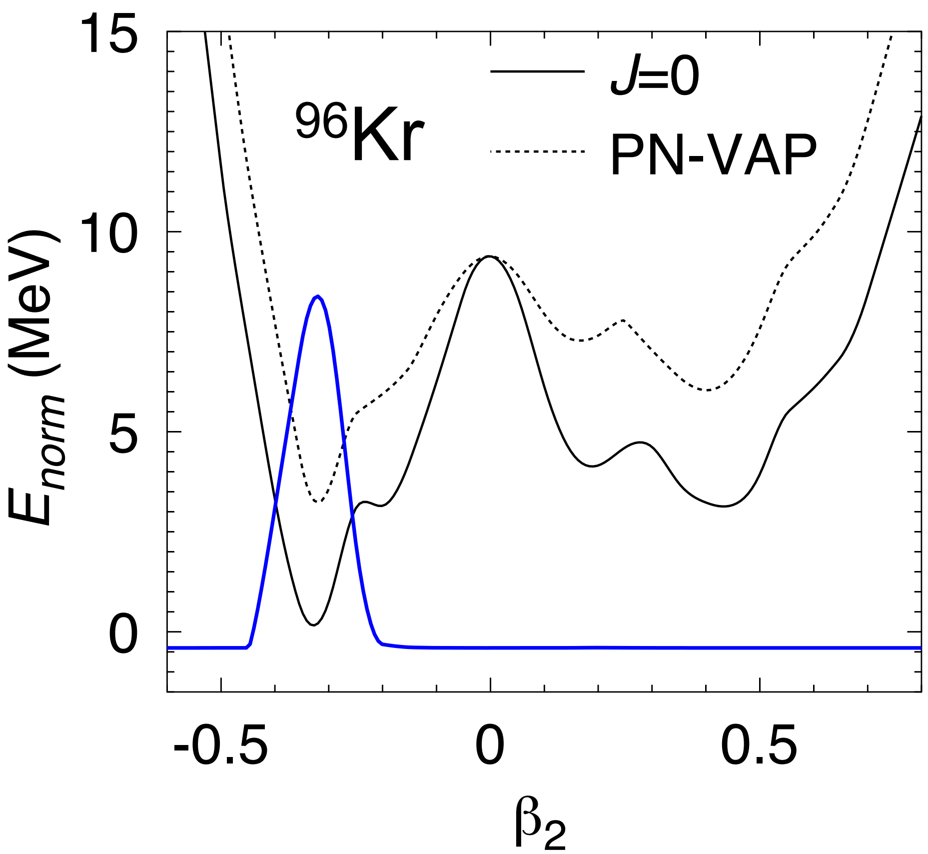

✓ The spherical shells are filled in or emptying depending on the deformation.

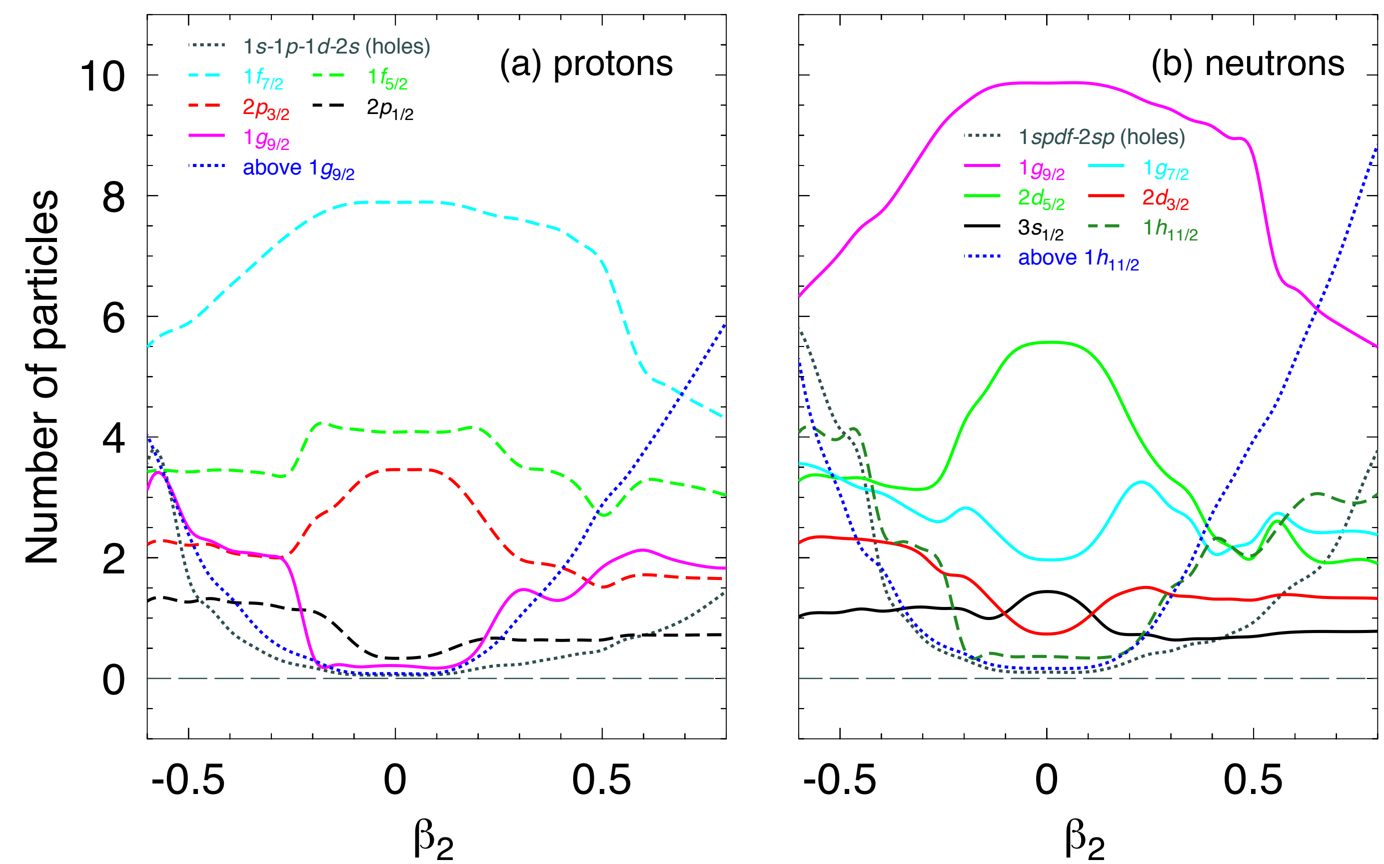

✓ The final occupation of each shell corresponding to a many-body state is computed with the GCM wave functions.

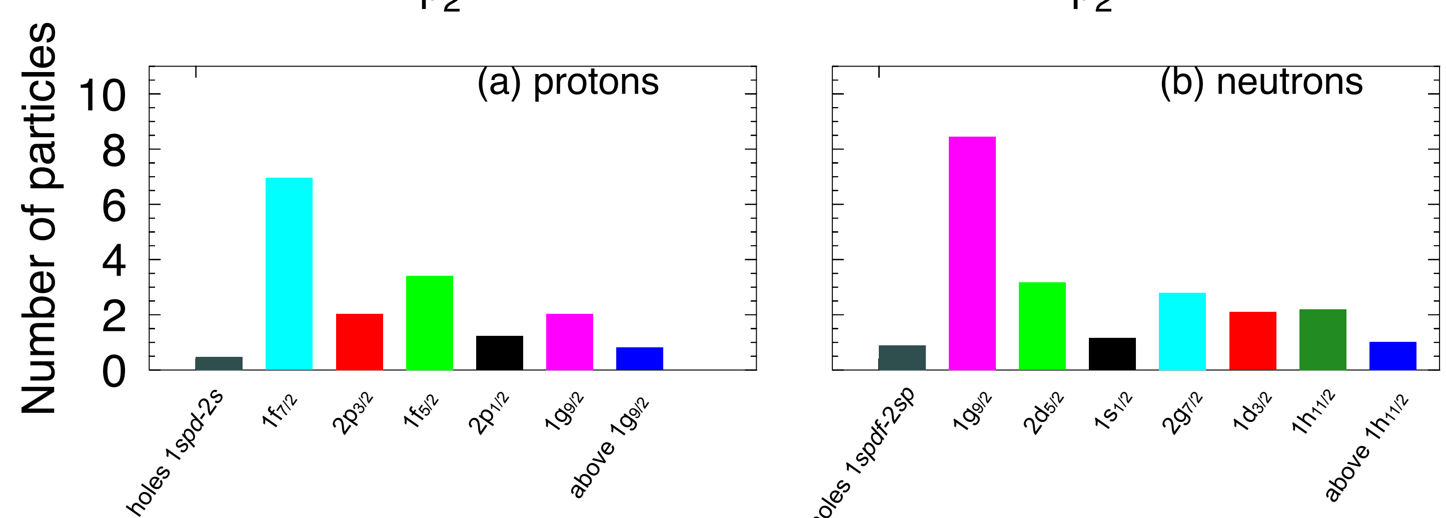

T. R. R., in preparation

Summary

- Experimental data are already able to constrain very long lower limit half-lives (we cross fingers for a positive signal soon!).

- 0νββ preferred mechanism is the exchange of a light Majorana neutrino but some other mechanisms are being considered too.

- NMEs differ a factor of three between the different methods but we need to understand which are the pros/cons of each method to provide reliable numbers (precision vs. accuracy).

- Nuclear physics aspects like deformation, pairing, shell effects, etc., are understood similarly within different approaches.

- Systematic comparisons between ISM/EDF methods have been performed.

Outlook

Additional (collective) degrees of freedom

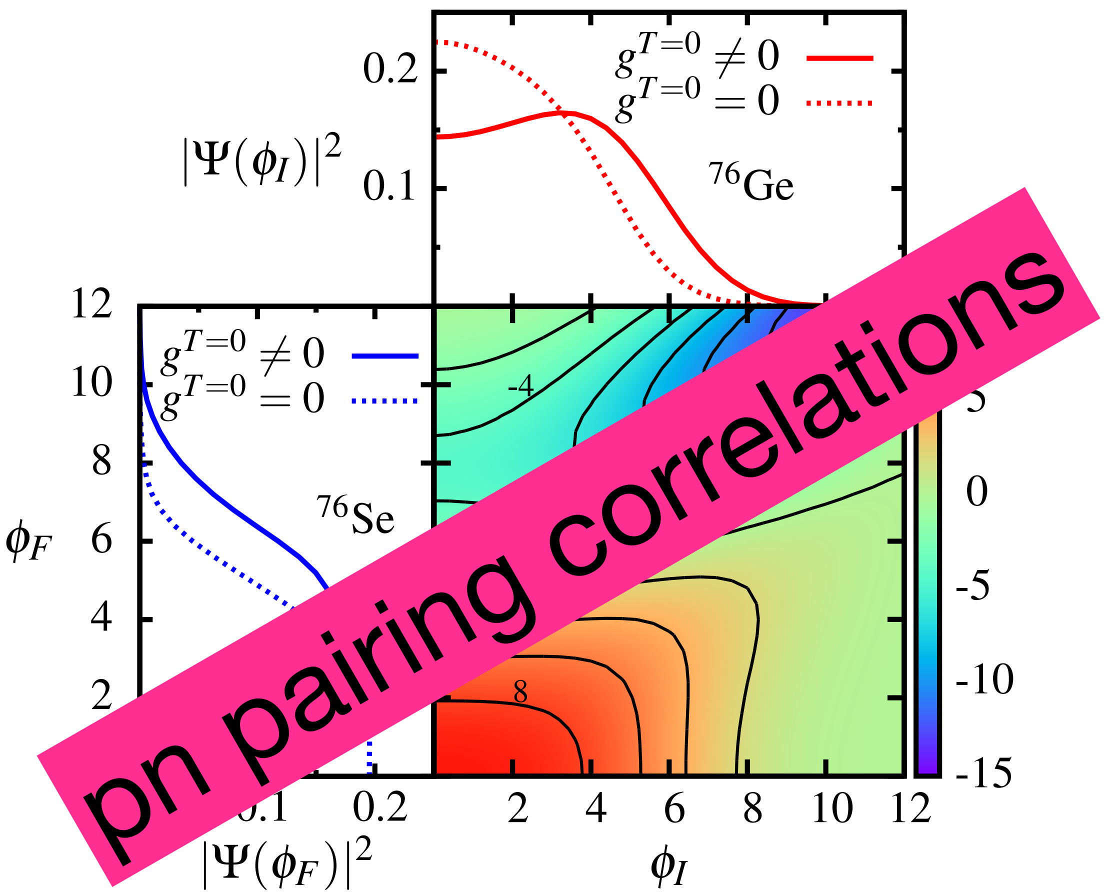

FIG. 3. (Color online.) **Bottom right:** $\mathcal{N}_{\phi_I}\mathcal{N}_{\phi_F}\langle\phi_F|\mathcal{P}_F\hat{M}_{0\nu}\mathcal{P}_I|\phi_I\rangle$ for projected quasiparticle vacua with different values of the initial and final isoscalar pairing amplitudes ϕ_I and ϕ_F, from the SkO′-based interaction (see text). **Top and bottom left:** Square of collective wave functions in ^{76}Ge and ^{76}Se.

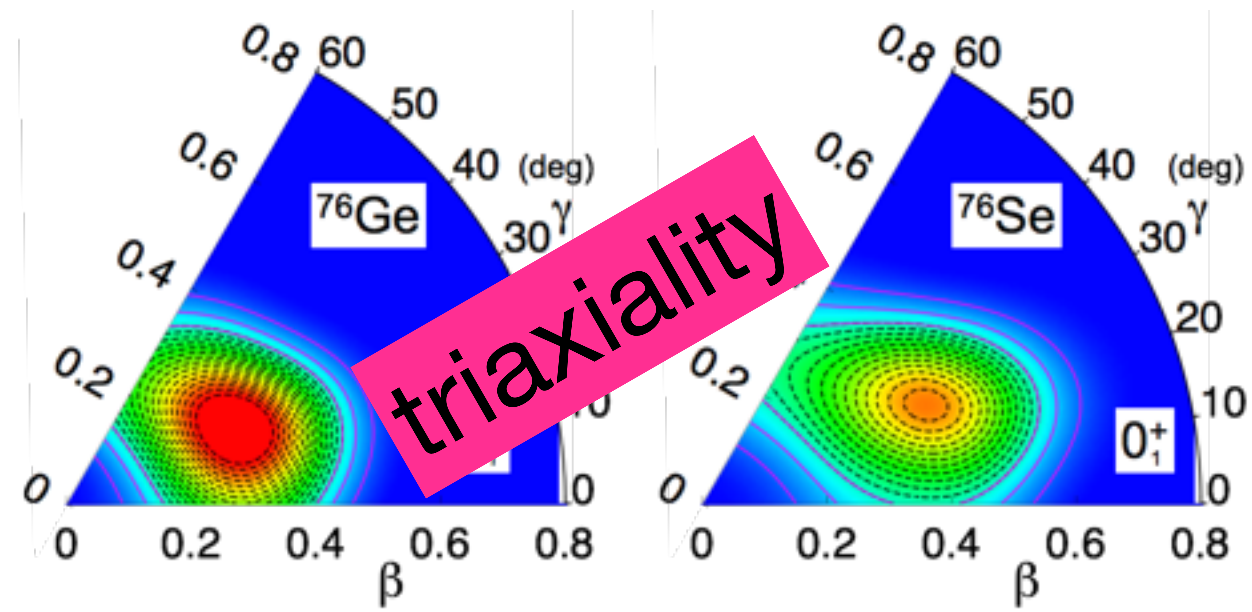

Outlook

Additional (non-collective) degrees of freedom

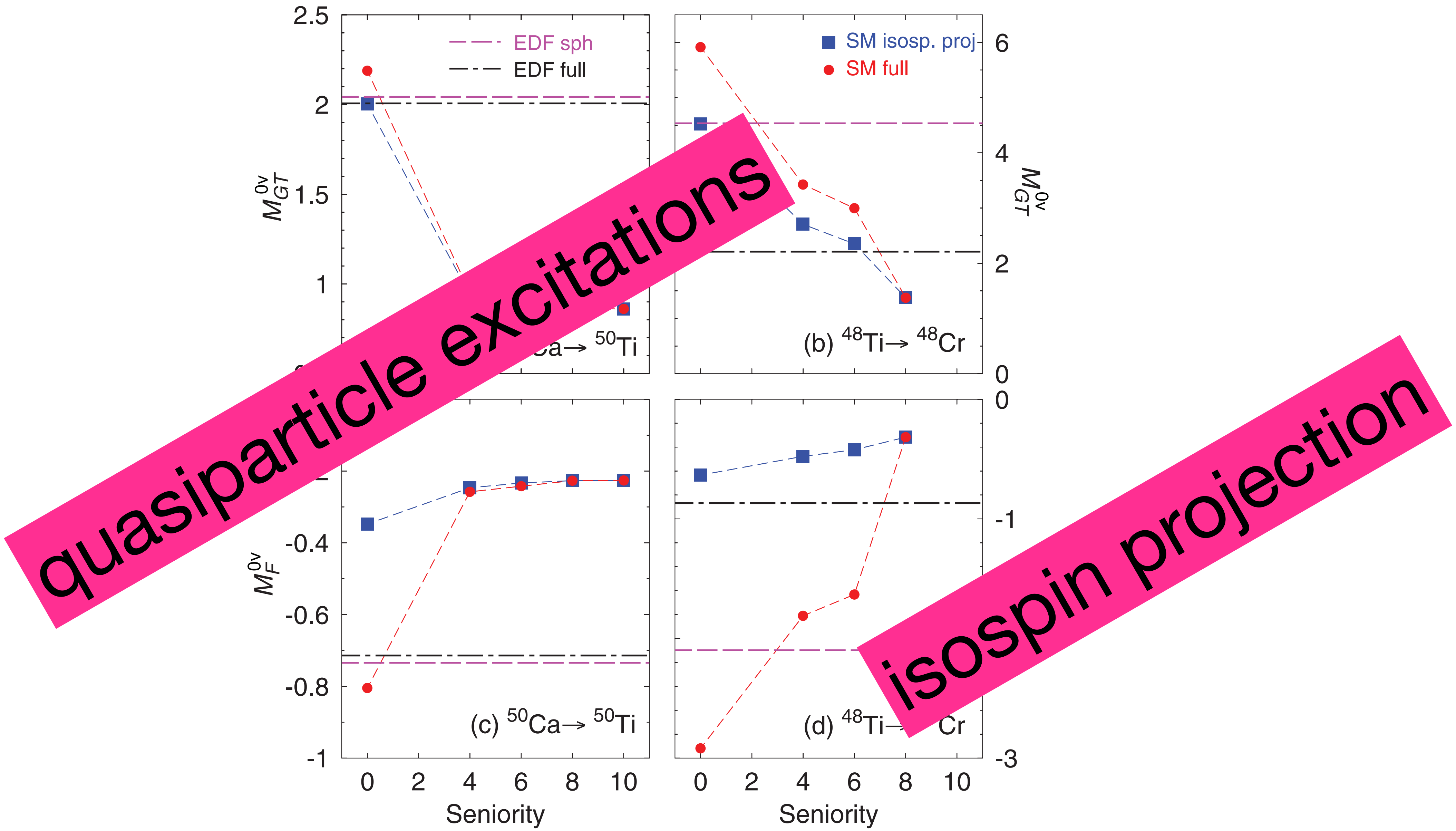

Outlook

Description of odd nuclei

2νββ-NMEs

TABLE III. Effective nuclear matrix elements ($M^{2\nu}_{eff}$) for $2\beta(2\nu)$-decay from the present work, ITEP evaluation, large-scale shell-model and QRPA calculations.

Parent nuclide	Process	Transition	Present work	Yale & ITEP [35, 38]	Shell model [42]	QRPA [43]
^{48}Ca	$2\beta^-$	$0^+ \to 0^+$	0.0383±0.0025	0.038±0.003	0.0389,0.0397,0.0538	0.0373
^{76}Ge	$2\beta^-$	$0^+ \to 0^+$	0.120±0.021	0.118±0.005	0.0961	0.147
^{82}Se	$2\beta^-$	$0^+ \to 0^+$	0.0826±0.0034	0.083±0.004	0.104	[illegible]
^{96}Zr	$2\beta^-$	$0^+ \to 0^+$	0.0824±0.0050	0.080±0.004		[illegible]
^{100}Mo	$2\beta^-$	$0^+ \to 0^+$	0.208±0.007	0.206±0.007		
^{100}Mo	$2\beta^-$	$0^+ \to 0^+_1$	0.170±0.020	0.167±0.011		
^{116}Cd	$2\beta^-$	$0^+ \to 0^+$	0.112±0.005	0.114±0.005		
^{128}Te	$2\beta^-$	$0^+ \to 0^+$	0.0326±0.0093	0.044±0.006	0.0489,0.0306	
^{130}Te	$2\beta^-$	$0^+ \to 0^+$	0.0303±0.0022	0.031±0.004	0.0356,0.0224	[illegible]
^{136}Xe	$2\beta^-$	$0^+ \to 0^+$	0.0173±0.0005		0.0207	
^{130}Ba	2ϵ	$0^+ \to 0^+$	0.218±0.062	0.174±0.017		
^{150}Nd	$2\beta^-$	$0^+ \to 0^+$	0.0572±0.0015	0.058±0.004		0.0348
^{150}Nd	$2\beta^-$	$0^+ \to 0^+_1$	0.0417±0.0063	0.042±0.006		
^{238}U	$2\beta^-$	$0^+ \to 0^+$	0.185±0.028	0.19±0.04		

Closure approximation

	Pure closure	Run[illegible]	[illegible]re	Mixed
$M^{0\nu}_{GT}$	2.750	[illegible]	[illegible]	2.983
$M^{0\nu}_{F}$	-0.60[illegible]	[illegible]	-0.620	-0.632
$M^{0\nu}_{T}$	[illegible]	[illegible]	-0.007	-0.011
$M^{0\nu}$	[illegible]	[illegible]35	3.285	3.377

[illegible] for the $0\nu\beta\beta$ decay of ^{82}Se (light neutrino e[illegible] calculated within different approximations. All calcu[illegible]s were done with CD-Bonn SRC parametrization and for the average closure energy $\langle E\rangle = 10.08$ MeV. The difference between mixed and pure closure total NME is about 8%.

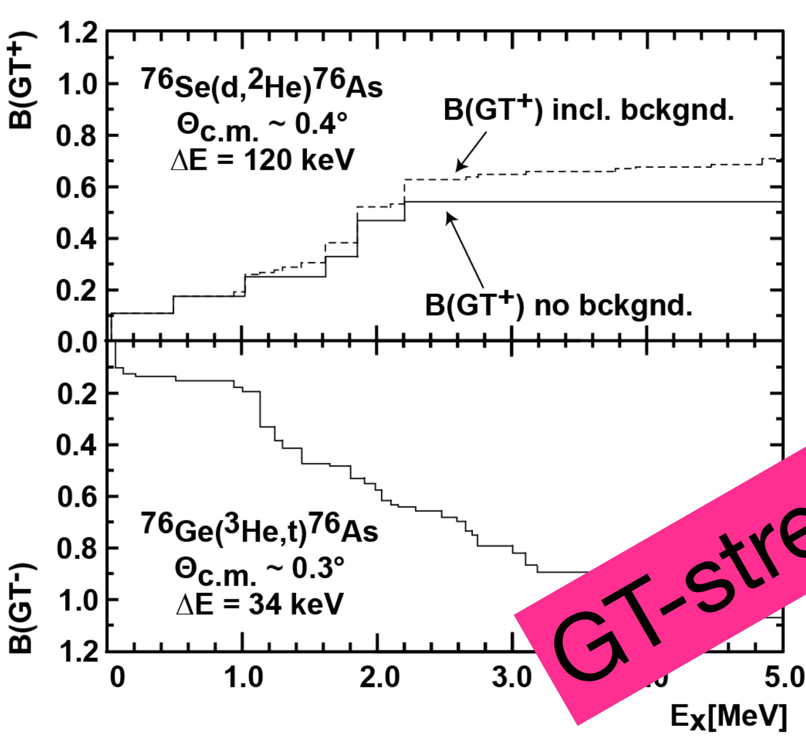

GT-strength

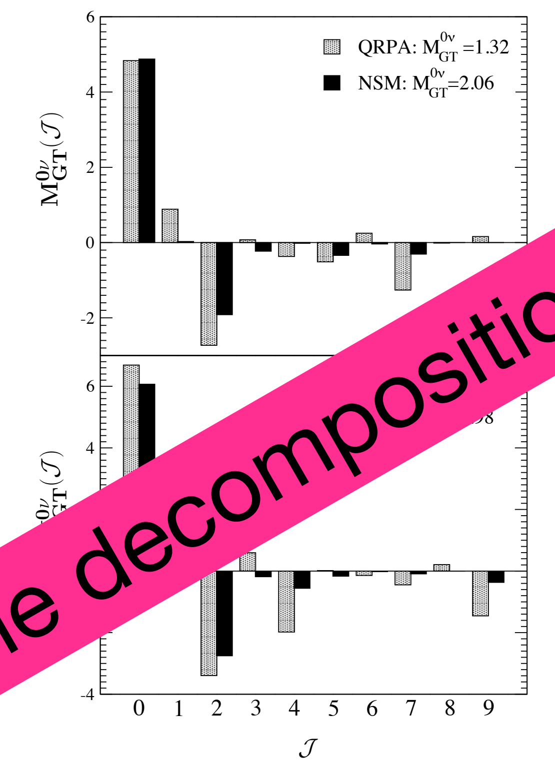

Multipole decomposition